



Technical Note

The IWG7 4MOST Galactic Pipeline (4GP): Development Report 3

Document No.: MST-TNO-XXX-YYYYY-GGGG-HHHH

Issue No.: 1.00

DocuShare Document URL: <https://ds-web.aip.de/docushare/dsweb/Services/Document-ZZZZ>

Prepared by

2018-06-11

Dominic Ford



Doc. Title: The IWG7 4MOST Galactic Pipeline (4GP): Development Report 3	
Doc no.: MST-TNO-XXX-YYYYY-GGGG-HHHH	
Issue no.: 1.00	Date: 2018-06-11
Document status	Page 2 of 40

Change Record

Issue	Date	Page, Section, Paragraph Affected	Reason, Remarks
1.00	2018-06-11	All	First version of document

List of Contributors

Name	First Name	Institute	Comments
Ford	Dominic	Lund Observatory	Lead Developer
Church	Ross	Lund Observatory	
Battistini	Chiara	Zentrum für Astronomie, Heidelberg	
Skuladottir	Ása	Max-Planck-Institut für Astronomie, Heidelberg	
Kordopatis	Georges	Observatoire de la Côte d'Azur, Nice	IWG7 Lead
Lind	Karin	Max-Planck-Institut für Astronomie, Heidelberg	IWG7 Lead
Feltzing	Sofia	Lund Observatory	



Doc. Title: The IWG7 4MOST Galactic Pipeline (4GP):	
Development Report 3	
Doc no.: MST-TNO-XXX-YYYYY-GGGG-HHHH	
Issue no.: 1.00	Date: 2018-06-11
Document status	Page 3 of 40

Table of contents

1	Scope	5
2	Applicable Documents (AD)	5
3	Reference Documents (RD).....	5
4	Introduction.....	6
4.1	The 4MOST Galactic Pipeline (4GP).....	6
4.2	The Cannon	7
4.2.1	Choice of parameters	7
4.2.2	Masking scheme.....	8
5	The training and test samples.....	8
5.1	Stellar parameters and abundances	8
5.2	Preparation of training spectra	11
5.3	Preparation of test spectra.....	11
6	Improvement in precision since 2017 December.....	11
7	Robustness against reddened spectra	15
8	Robustness against residual radial velocities	19
9	Robustness against sky contamination.....	21
10	Conclusions and perspectives	24
	Appendix A : Mapping performance across the HR diagram (LRS)	26
A. 1	T_{eff}	26
A. 2	$\log(g)$	26
A. 3	[Fe/H]	27
A. 4	[Ca/H].....	27
A. 5	[Mg/H].....	28
A. 6	[Ti/H].....	28
A. 7	[Si/H]	29
A. 8	[Na/H].....	29
A. 9	[Ni/H]	30
A. 10	[Cr/H]	30
	Appendix B : Mapping performance across the HR diagram (HRS).....	31
B. 1	T_{eff}	31
B. 2	$\log(g)$	31
B. 3	[Fe/H].....	32



Doc. Title: The IWG7 4MOST Galactic Pipeline (4GP):	
Development Report 3	
Doc no.: MST-TNO-XXX-YYYYY-GGGG-HHHH	
Issue no.: 1.00	Date: 2018-06-11
Document status	Page 4 of 40

B. 4 [Ca/H]	32
B. 5 [Mg/H]	33
B. 6 [Ti/H]	33
B. 7 [Si/H]	34
B. 8 [Na/H]	34
B. 9 [Ni/H]	35
B. 10 [Cr/H]	35
Appendix C Line list	36
Appendix D List of Acronyms	40

List of Figures

Figure 5-1: The distribution of T_{eff} values in the GALAH sample (12,626 stars)	9
Figure 5-2: The distribution of $\log(g)$ values in the GALAH sample (12,626 stars)	10
Figure 5-3: The distribution of [Fe/H] values in the GALAH sample (12,626 stars)	10
Figure 5-4: The distribution of stellar parameters in the GALAH sample (12,626 stars). Stars are colour-coded by metallicity.	11
Figure 6-1: The RMS offsets in T_{eff} and $\log(g)$ for giants and dwarfs in four metallicity bins, based on synthetic LRS observations	12
Figure 6-2: The RMS offsets in T_{eff} and $\log(g)$ for giants and dwarfs in four metallicity bins, based on synthetic HRS observations	12
Figure 6-3: The RMS offsets in each abundance in four metallicity bins, for synthetic LRS observations	13
Figure 6-4: The RMS offset in each abundance in four metallicity bins, for synthetic HRS observations	14
Figure 7-1: The effect of reddening the solar spectrum, holding its intrinsic (unreddened) brightness constant at $g=15$. To enhance readability, the spectral resolution has been reduced to 250.	15
Figure 7-2: The effect of reddening the solar spectrum, holding its observed brightness constant at $g=15$. To enhance readability, the spectral resolution has been reduced to 250. ...	16
Figure 7-3: The wavelength-dependent signal-to-noise ratio of the solar spectrum, for simulated 4MOST exposures achieving an SNR/pixel of 50 in the window 6180 – 6680 Å..	17
Figure 7-4: The RMS offset in each parameter as a function of $E(B-V)$, for synthetic observations with $\text{SNR}/\text{pixel}=50$	18
Figure 8-1: The RMS offset in each parameter when uncorrected radial velocities are introduced into the test spectra, for synthetic observations with $\text{SNR}/\text{pixel}=50$	20
Figure 9-1: Kiel diagrams mapping of offsets in the Cannon's determinations of T_{eff} and $\log(g)$. The colour of each point shows the offset in $\log(g)$; the size of each point shows the offset in T_{eff} . See the text for full details.	22
Figure 9-2: Kiel diagrams mapping of offsets in the Cannon's determinations of [Fe/H]. The	



Doc. Title: The IWG7 4MOST Galactic Pipeline (4GP): Development Report 3	
Doc no.: MST-TNO-XXX-YYYYY-GGGG-HHHH	
Issue no.: 1.00	Date: 2018-06-11
Document status	Page 5 of 40

colour of each point shows the value of [Fe/H] used to synthesise each spectrum; the size of each point shows the offset in the Cannon's determination of [Fe/H]. See the text for full details.....	23
Figure 9-3: Offsets in the Cannon's determinations of the abundances of individual elements.	24

List of Tables

Table 10-1 Line list from Ruchti et al. (2015) [RD6].....	39
---	----

1 Scope

We present an update on IWG7's development of a spectral analysis pipeline for the 4MOST Galactic Surveys.

2 Applicable Documents (AD)

The following applicable documents (AD) of the exact issue shown form a part of this document to the extent described herein. In the event of conflict between the documents referenced herein and the contents of this document, the contents of this document are the superseding requirement.

AD ID	Document Title	Document Number	Issue	Date
[AD1]	IWG7 Management Plan	MST-PLA-PSC-20307-09237-0001	0.07	05.01.2017

3 Reference Documents (RD)

The following reference documents (RD) contain useful information relevant to the subject of the present document.

RD ID	Document Title	Document Number	Issue	Date
[RD1]	Casey, A. et al. 2016 – http://adsabs.harvard.edu/abs/2016arXiv160303040C			
[RD2]	Preliminary Results of IWG7 for radial velocities, atmospheric parameters and chemical abundances (Kordopatis et al. 2016)			
[RD3]	Ford, D. 2017a, The IWG7 4MOST Galactic Pipeline (4GP): Development Report (July 2017)			
[RD4]	Ford, D. 2017b, The IWG7 4MOST Galactic Pipeline (4GP): Development Report 2 (December 2017)			



Doc. Title: The IWG7 4MOST Galactic Pipeline (4GP): Development Report 3	
Doc no.: MST-TNO-XXX-YYYYY-GGGG-HHHH	
Issue no.: 1.00	Date: 2018-06-11
Document status	Page 6 of 40

RD ID	Document Title	Document Number	Issue	Date
[RD5]	Ness, M. et al. 2015, ApJ, 808, 16 – http://adsabs.harvard.edu/abs/2015ApJ...808...16N			
[RD6]	Ruchti G. et al. 2016, MNRAS, 461, 2174 – http://adsabs.harvard.edu/abs/2016ascl.soft06001R			
[RD7]	Gustafsson B. et al. 2008, A&A, 486, 951 – http://adsabs.harvard.edu/abs/2008A%26A...486..951G			
[RD8]	Buder S. et al. 2018, MNRAS – http://adsabs.harvard.edu/doi/10.1093/mnras/sty1281			
[RD9]	Cardelli et al., ApJ 345, 245 (1989)			

4 Introduction

The analysis of observations from large spectroscopic surveys poses a substantial computational challenge. Multi-object spectrographs such as 4MOST can observe thousands of objects in a single pointing. It is infeasible to propose doing manual abundance analysis on more than a tiny proportion of these stars. By contrast, machine learning has emerged as a technique which scales affordably to such large data volumes.

Previously, we presented proof-of-principle tests to demonstrate that machine-learning techniques can deliver abundances to the accuracy required by the Surveys – as set out in the IWG7 Management Plan [AD1] – albeit in highly idealised test conditions using synthetic spectra (Ford et al. 2017a [RD3]; Ford et al. 2017b [RD4]).

In this report, we develop these tests further to demonstrate the robustness of machine-learning techniques against a variety of imperfections in the test spectra:

- Reddening
- Residual uncorrected radial velocities
- Sky contamination

As in our previous report, we test only one machine-learning technique – the Cannon (Ness et al. 2015 [RD5]). However, the framework we have developed for performing these tests is highly flexible and could be used to test other algorithms also. We anticipate that it is very likely that improved algorithms will become available by the time 4MOST begins observing.

4.1 The 4MOST Galactic Pipeline (4GP)

The framework we use in this report is the 4MOST Galactic Pipeline (4GP). This is a collection of Python modules which use a common data format to store and manipulate spectra and their associated metadata (Ford et al. 2017b [RD4]).



Doc. Title: The IWG7 4MOST Galactic Pipeline (4GP):	
Development Report 3	
Doc no.: MST-TNO-XXX-YYYYY-GGGG-HHHH	
Issue no.: 1.00	Date: 2018-06-11
Document status	Page 7 of 40

The framework is available in two repositories on GitHub. The first repository contains the Python modules which provide programmatic interfaces for creating and manipulating libraries of spectra, including wrappers for passing them to various analysis tools:

<https://github.com/dcf21/4most-4gp>

The second repository contains python scripts which utilise these modules to synthesise the spectra and perform the tests described in this report:

<https://github.com/dcf21/4most-4gp-scripts>

Step-by-step instructions for installing and running 4GP can be found in the Wiki pages on GitHub:

<https://github.com/dcf21/4most-4gp/wiki>

<https://github.com/dcf21/4most-4gp-scripts/wiki>

4.2 The Cannon

The Cannon analyses spectra by forming an internal model of how the continuum-normalised flux in each pixel i within a spectrum can be expressed as a quadratic polynomial function of the N parameters being fitted. For example, the expression for the flux f_i in pixel i might include the terms

$$f_i = a_0 + a_1 T_{\text{eff}} + a_2 \log(g) + a_3 [\text{Fe}/\text{H}] + \dots + a_n T_{\text{eff}} \log(g) + \dots + \text{noise} \quad [1]$$

These expressions include one constant offset (a_0), N terms which are linear in each parameter, and $N(N+1)/2$ quadratic terms which contain every possible product of pairs of parameters.

The coefficients a_j are unique to every pixel in the spectrum, which are described by different polynomials. In our tests, these coefficients are determined by fitting to a sample of 3,052 synthetic training spectra (see Section 5) whose stellar parameters, abundances and fluxes are all known.

In the subsequent tests, the Cannon performs a weighted least-squares search for the stellar parameters and abundances which best match the fluxes within each test spectrum.

4.2.1 Choice of parameters

In all the tests described in this report, the Cannon fits ten parameters: T_{eff} , $\log(g)$, $[\text{Fe}/\text{H}]$, $[\text{Ca}/\text{H}]$, $[\text{Mg}/\text{H}]$, $[\text{Ti}/\text{H}]$, $[\text{Si}/\text{H}]$, $[\text{Na}/\text{H}]$, $[\text{Ni}/\text{H}]$, $[\text{Cr}/\text{H}]$. The polynomials consequently contain 10 linear terms and 55 quadratic terms for each pixel.



Doc. Title: The IWG7 4MOST Galactic Pipeline (4GP):	
Development Report 3	
Doc no.: MST-TNO-XXX-YYYYY-GGGG-HHHH	
Issue no.: 1.00	Date: 2018-06-11
Document status	Page 8 of 40

4.2.2 Masking scheme

Masking the spectra, such that the Cannon only fits lines which are known to be reliable, reduces the risk of the Cannon learning to use weak lines which may be undetectable in noisy spectra. In our previous report (Ford et al. 2017b [RD4]) we demonstrated that this significantly improves performance.

In all the tests described in this report, we create a mask based on the list of important lines compiled by Ruchti et al. (2016) [RD6], which is reproduced in Appendix C. We only allow the Cannon to see pixels in windows extending 1 Å to either side of the lines associated with the elements whose abundances we are fitting.

Larger windows are created for H-alpha, between 6470 and 6650 Å, for the Mg B line between 5100 and 5250 Å, and for the Ca I lines between 6152 and 6172 Å. The latter two regions are important indicators for $\log(g)$.

5 The training and test samples

In this report we use different and improved training spectra from our previous report. For a summary of the changes, see Section 6.

Until 4MOST is operational, we do not have observed spectra which match 4MOST’s wavelength span and resolution. Consequently, to run tests on the wavelength bands in which 4MOST will observe, we are restricted to using synthetic spectra.

We create these spectra using Turbospectrum with MARCS model atmospheres (Gustafsson et al. 2008 [RD7]) and VALD line lists provided by Bengt Edvardsson (private communication).

We simulate 4MOST’s wavelength-dependent sensitivity using the 4MOST Facility Simulator (4FS). We configure 4FS to inject a variable amount of noise into each spectrum, which we quantify by the median SNR/pixel in the window 6180 – 6680 Å. This continuum window is selected because it is within the wavelength range of both LRS and HRS.

Spectra are produced for both 4MOST LRS and HRS and tested separately. In both cases, we stitch the three arms of the 4MOST spectrographs into a single spectrum for simultaneous analysis by the Cannon.

5.1 Stellar parameters and abundances

A good set of training / test spectra needs to sample all the regions of parameter space in which 4MOST targets will lie. To create such a sample, with a physically realistic distribution of stellar parameters and abundances, we take parameter values from the training catalogue used in GALAH DR2 (Buder et al. 2018 [RD8]). To the 10,605 training spectra used in GALAH DR2, we add objects which were rejected from the final GALAH training set because they have “flagged” parameters, meaning that their quoted abundances may be upper limits (Karin Lind, private communication). This boosts the number of low-metallicity stars in the sample and yields a sample of 12,626 stars.



Doc. Title: The IWG7 4MOST Galactic Pipeline (4GP):	
Development Report 3	
Doc no.: MST-TNO-XXX-YYYYY-GGGG-HHHH	
Issue no.: 1.00	Date: 2018-06-11
Document status	Page 9 of 40

The use of flagged objects in our sample is expected to have minimal effect on our results, since we do not use the GALAH spectra, but only the parameter values to synthesise our own spectra. The only implication of using flagged abundances in our tests is that it modifies the distribution of abundances we test.

To create training and test samples, we divide the sample of 12,626 stars such that 25% are used as a training sample (3,052 stars), and the remaining 75% are used as test objects (9,574 stars).

The distribution of their stellar parameters is shown in Figure 5-1, Figure 5-2 and Figure 5-3.

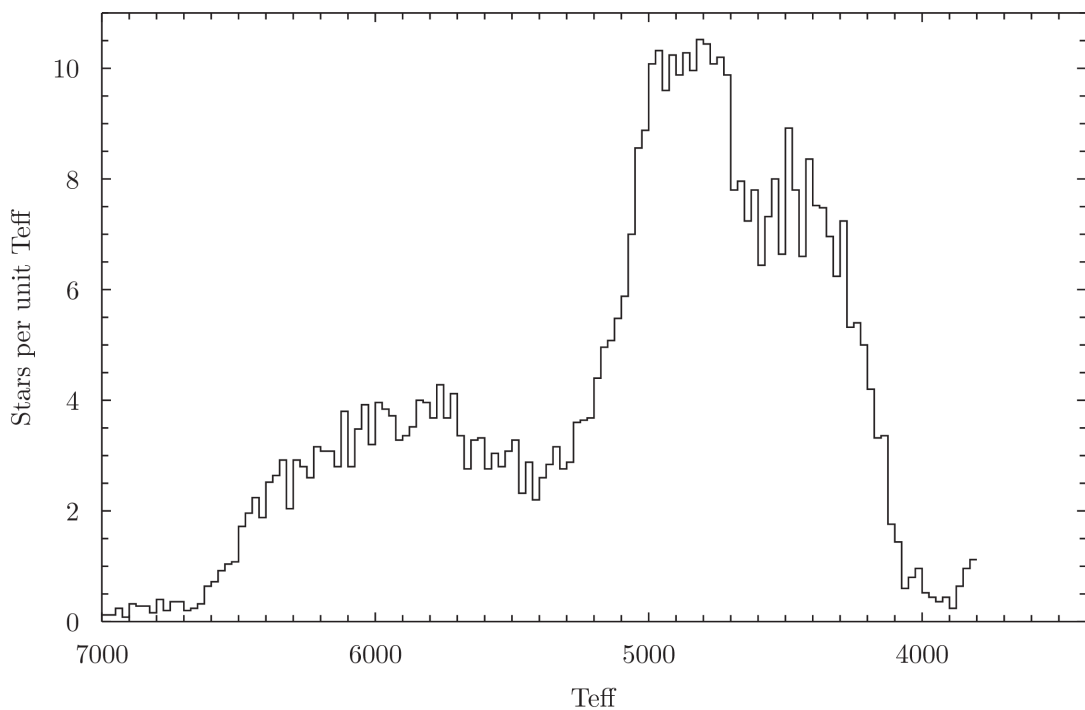


Figure 5-1: The distribution of T_{eff} values in the GALAH sample (12,626 stars).



Doc. Title: The IWG7 4MOST Galactic Pipeline (4GP):	
Development Report 3	
Doc no.: MST-TNO-XXX-YYYYY-GGGG-HHHH	
Issue no.: 1.00	Date: 2018-06-11
Document status	Page 10 of 40

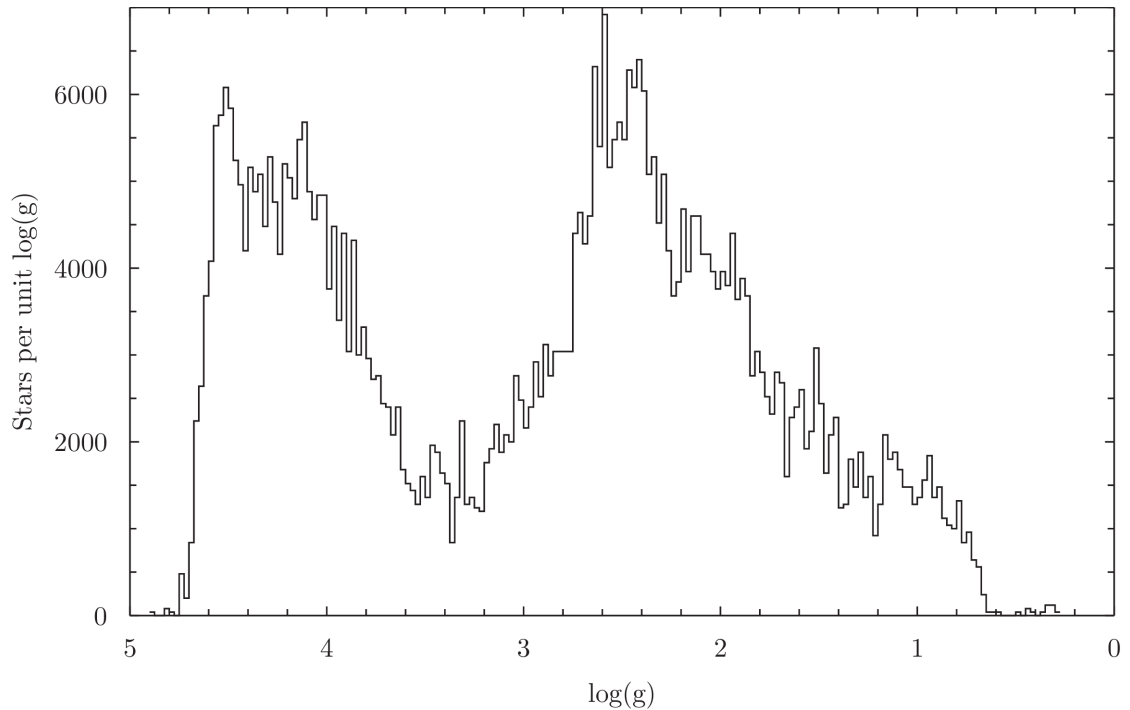


Figure 5-2: The distribution of $\log(g)$ values in the GALAH sample (12,626 stars).

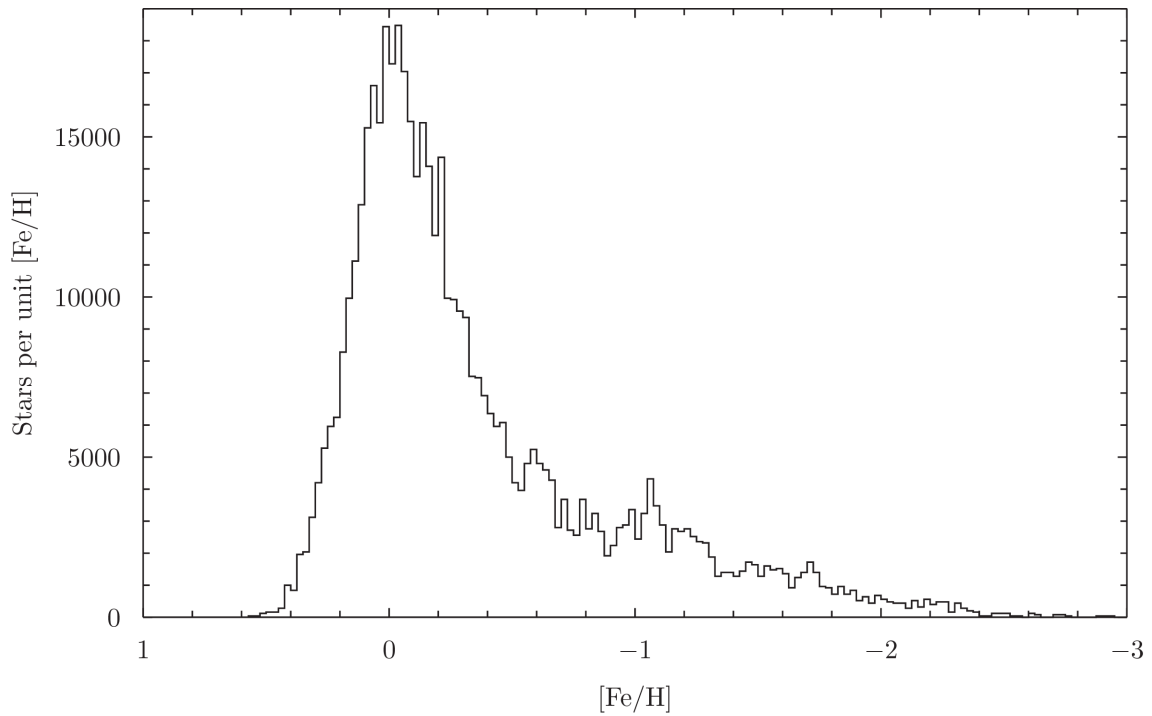


Figure 5-3: The distribution of [Fe/H] values in the GALAH sample (12,626 stars).



Doc. Title: The IWG7 4MOST Galactic Pipeline (4GP):	
Development Report 3	
Doc no.: MST-TNO-XXX-YYYYY-GGGG-HHHH	
Issue no.: 1.00	Date: 2018-06-11
Document status	Page 11 of 40

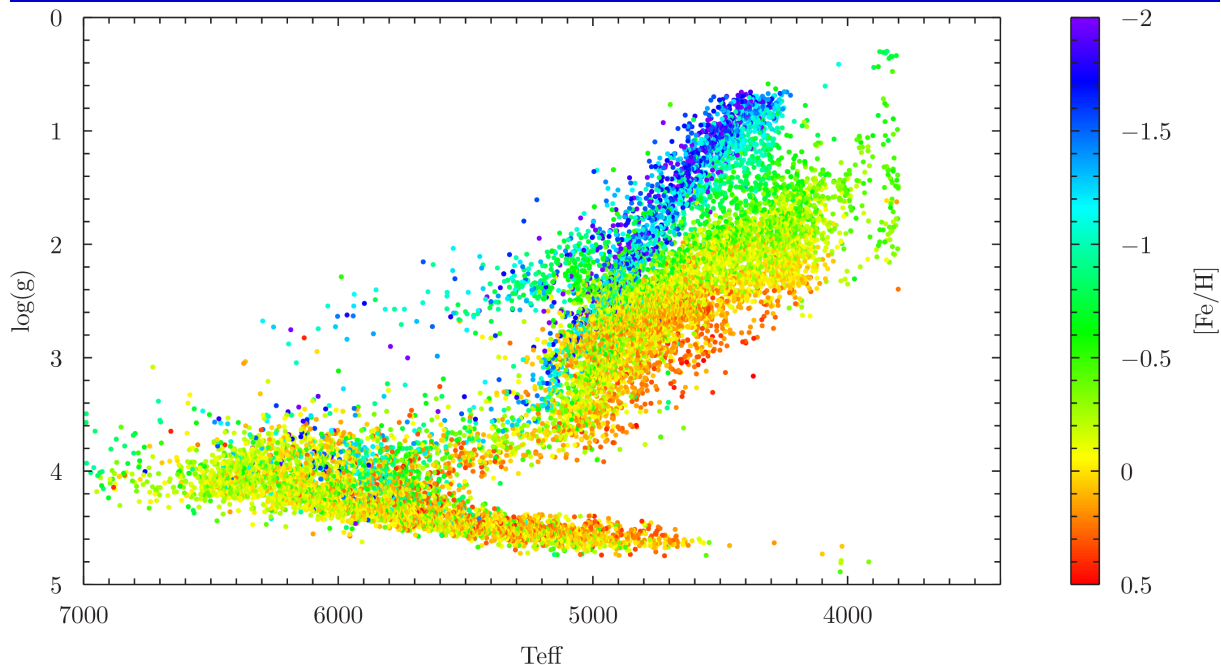


Figure 5-4: The distribution of stellar parameters in the GALAH sample (12,626 stars). Stars are colour-coded by metallicity.

5.2 Preparation of training spectra

We use 4FS to insert noise into our 3,052 training spectra such that they have a median SNR/pixel of 250 in the window 6180 – 6680 Å. This is preferable to training the Cannon on perfectly noiseless spectra, as it ensures that it does not learn to use any very weak lines which could never be observed in practice.

5.3 Preparation of test spectra

For most of the tests in this report, we use 4FS-ETC to insert noise into our 9,574 test spectra such that they have a median SNR/pixel of 50 in the window 6180 – 6680 Å. This is a noise level that we expect to be typical of the observations that 4MOST will make.

In Section 6, we show the precision that the Cannon achieves as a function of SNR. For these tests, we insert noise at a wide range of different noise levels.

6 Improvement in precision since 2017 December

The training and test samples described in Section 5 differ from our previous report, which used the stellar parameters and abundances of stars observed with UVES in the Gaia-ESO Data Release 5 (DR5) catalogue.

In our previous report, we created a test sample by adding random Gaussian-distributed perturbations with a standard deviation of 0.1 dex to each abundance. This smeared out the tight correlations between various abundances, in effect meaning that our test spectra sampled regions of abundance parameter space outside those sampled by the training spectra.



Doc. Title: The IWG7 4MOST Galactic Pipeline (4GP):	
Development Report 3	
Doc no.: MST-TNO-XXX-YYYYY-GGGG-HHHH	
Issue no.: 1.00	Date: 2018-06-11
Document status	Page 12 of 40

We believe that this significantly degraded the performance of the Cannon in our previous report and observe that it performs better with our new training and test samples. Consequently, in this section we repeat the most important plots from our previous report, using the new samples.

The plots below show the root mean square (RMS) offset in the Cannon's estimates of each stellar parameter and abundance, as compared to the values used to synthesise the test spectra, plotted as a function of the noise level of the input spectra. We split the test sample into giants and dwarfs along the line $\log(g) = 3.25$ and for consistency with previous reports, we express the SNR of each spectrum per Å in the window $6180 - 6680$ Å.

Horizontal grey lines in each plot show the target accuracies required by the IWG7 Management Plan [AD1].

In Appendices A and B we further analyse the Cannon's performance as a function of T_{eff} and $\log(g)$. We plot the test stars in a $T_{\text{eff}}\text{-}\log(g)$ plane, and colour code the lowest SNR at which the Cannon successfully extracts the parameters of each test star.

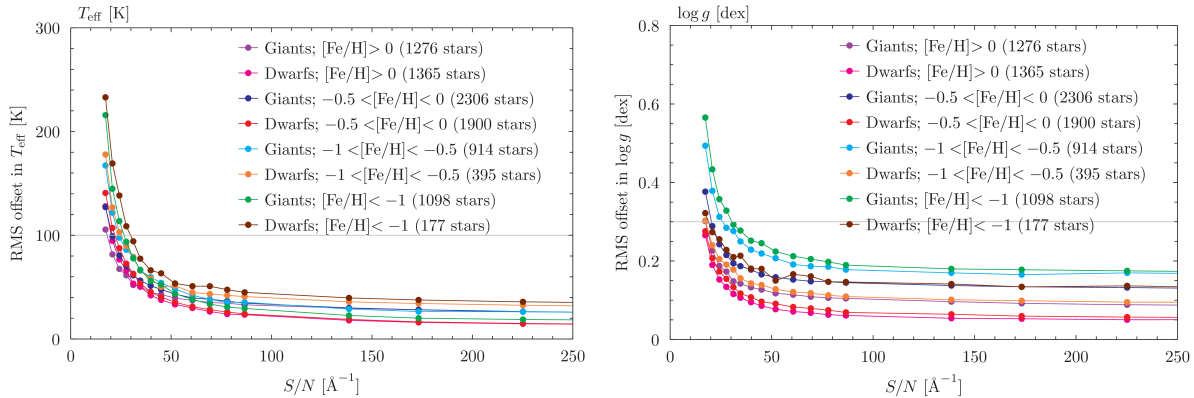


Figure 6-1: The RMS offsets in T_{eff} and $\log(g)$ for giants and dwarfs in four metallicity bins, based on synthetic LRS observations.

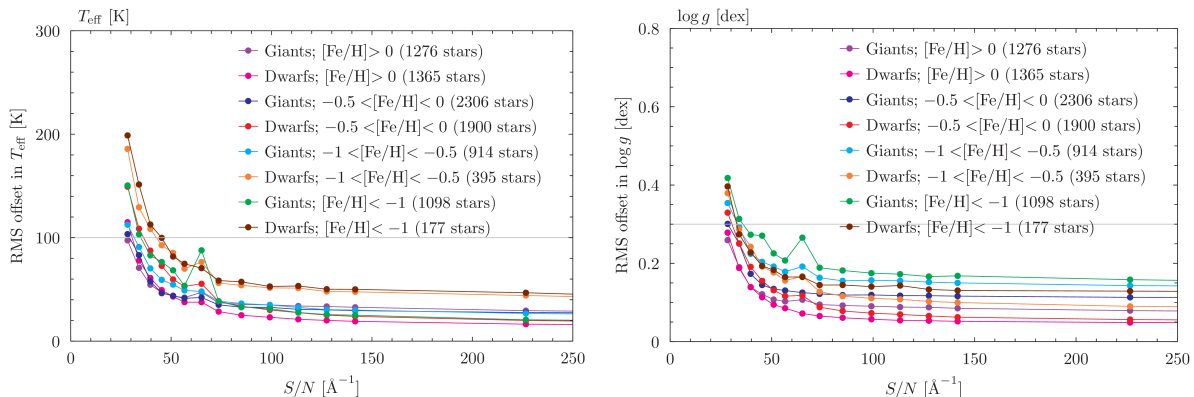


Figure 6-2: The RMS offsets in T_{eff} and $\log(g)$ for giants and dwarfs in four metallicity bins, based on synthetic HRS observations.



Doc. Title: The IWG7 4MOST Galactic Pipeline (4GP):	
Development Report 3	
Doc no.: MST-TNO-XXX-YYYYY-GGGG-HHHH	
Issue no.: 1.00	Date: 2018-06-11
Document status	Page 13 of 40

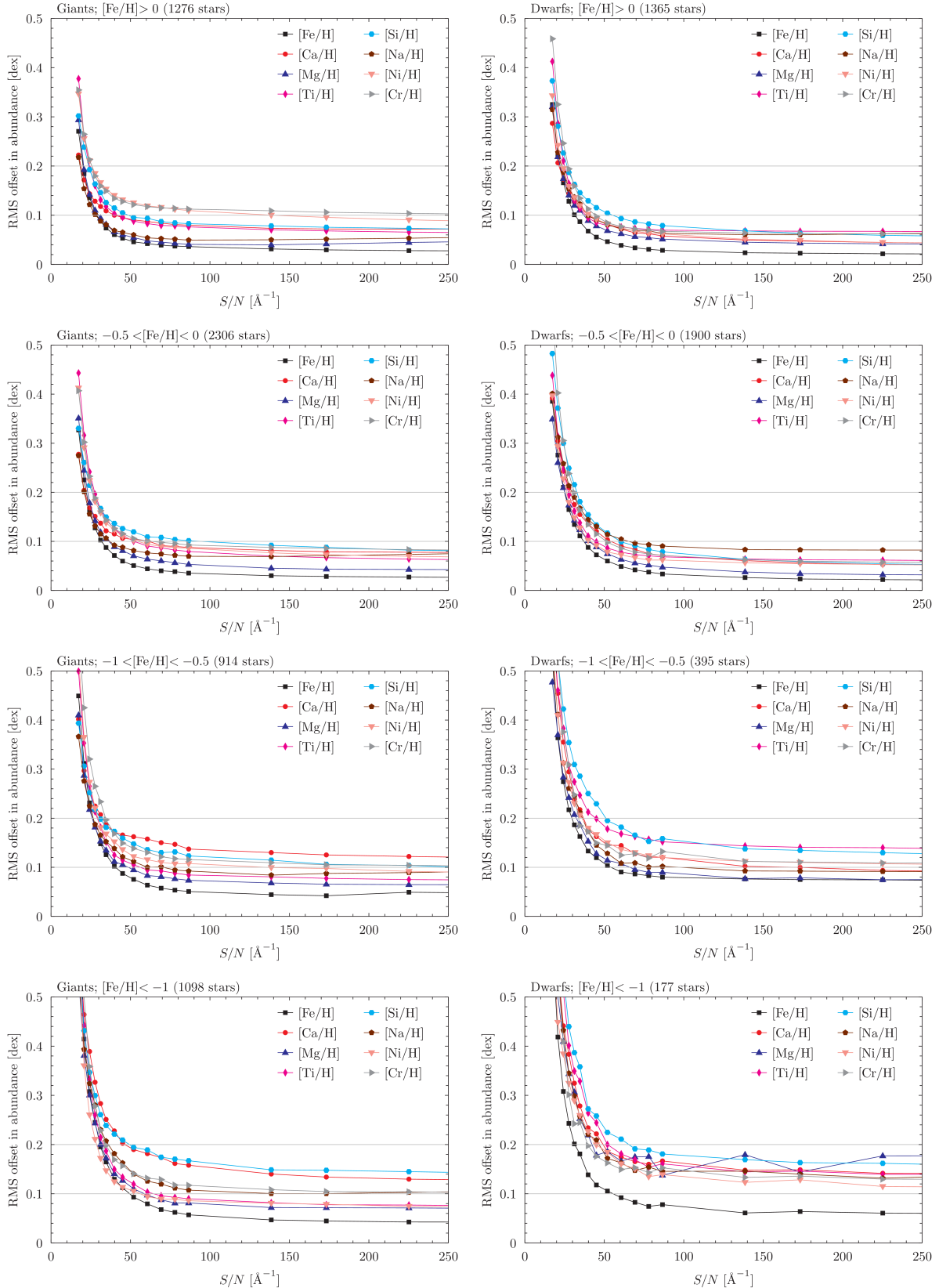


Figure 6-3: The RMS offsets in each abundance in four metallicity bins, for synthetic LRS observations.



Doc. Title: The IWG7 4MOST Galactic Pipeline (4GP): Development Report 3	
Doc no.: MST-TNO-XXX-YYYYY-GGGG-HHHH	
Issue no.: 1.00	Date: 2018-06-11
Document status	Page 14 of 40

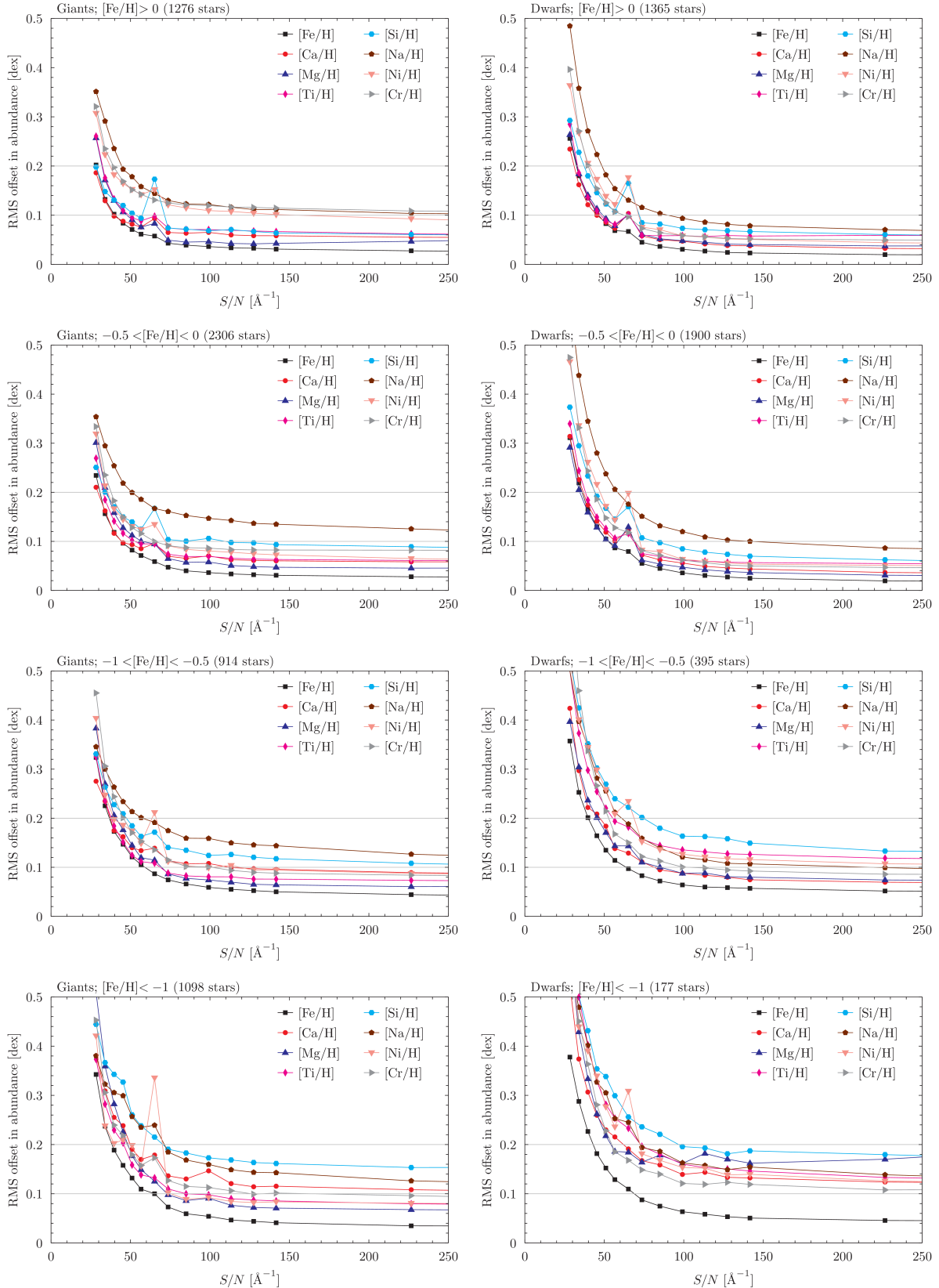


Figure 6-4: The RMS offset in each abundance in four metallicity bins, for synthetic HRS observations.



Doc. Title: The IWG7 4MOST Galactic Pipeline (4GP):	
Development Report 3	
Doc no.: MST-TNO-XXX-YYYYY-GGGG-HHHH	
Issue no.: 1.00	Date: 2018-06-11
Document status	Page 15 of 40

7 Robustness against reddened spectra

In this section we test the robustness of the Cannon to fitting reddened spectra, when it is trained on perfectly unreddened objects.

The training sample remains unchanged from the previous sections, but we apply reddening to the test spectra. The code used to apply the reddening can be found here:

https://github.com/dcf21/4most-4gp/blob/master/src/pythonModules/fourgp_degrade/fourgp_degrade/redden.py

We implement the reddening prescriptions from Cardelli et al. (1989) [RD9], as implemented by Ben Davies (private communication).

The effect of this reddening prescription is illustrated in Figure 7-1 for a low-resolution solar spectrum, holding the intrinsic unreddened brightness of the spectrum constant at SDSS g=15.

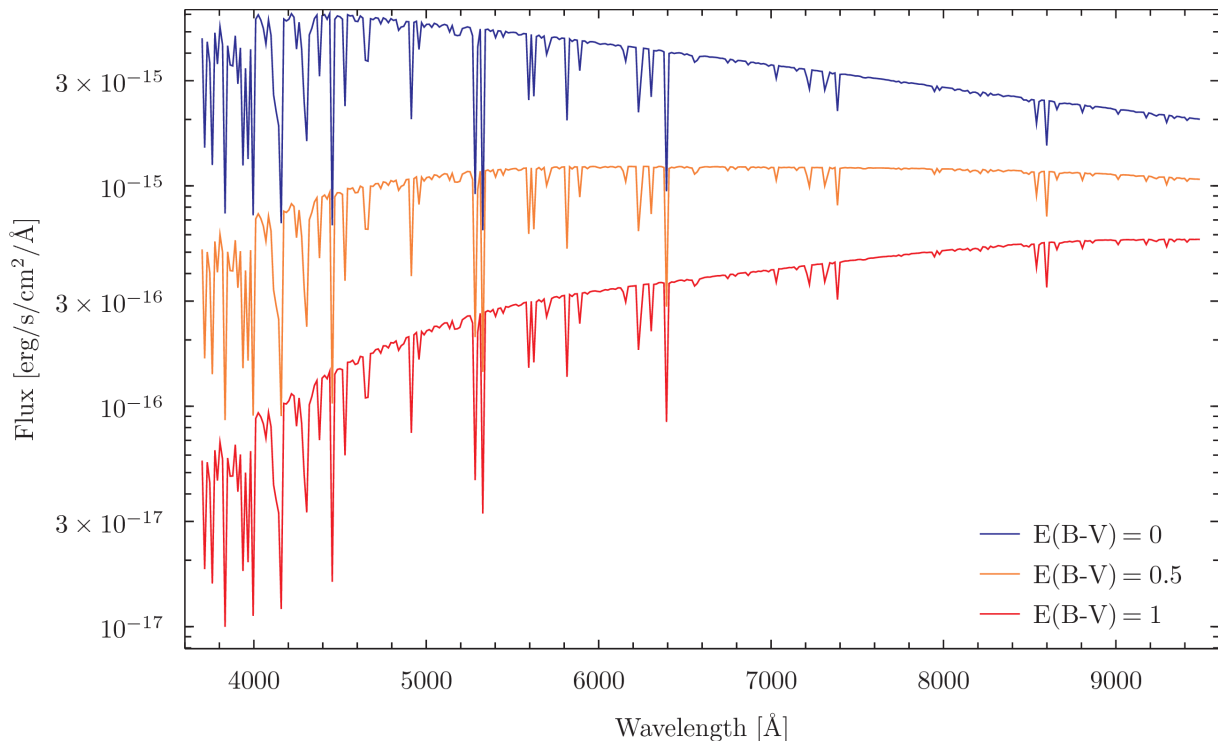


Figure 7-1: The effect of reddening the solar spectrum, holding its intrinsic (unreddened) brightness constant at g=15. To enhance readability, the spectral resolution has been reduced to 250.

In practice, however, 4MOST targets are selected on the basis of their observed magnitudes rather than their intrinsic magnitudes. Figure 7-2 shows the effect of reddening the same solar spectrum while holding its observed brightness constant at SDSS g=15. It should be noted that the exposure times for stars of equivalent g-band magnitude only increase dramatically with reddening if a high SNR is required in the far blue end of the spectrum.



Doc. Title: The IWG7 4MOST Galactic Pipeline (4GP):	
Development Report 3	
Doc no.: MST-TNO-XXX-YYYYY-GGGG-HHHH	
Issue no.: 1.00	Date: 2018-06-11
Document status	Page 16 of 40

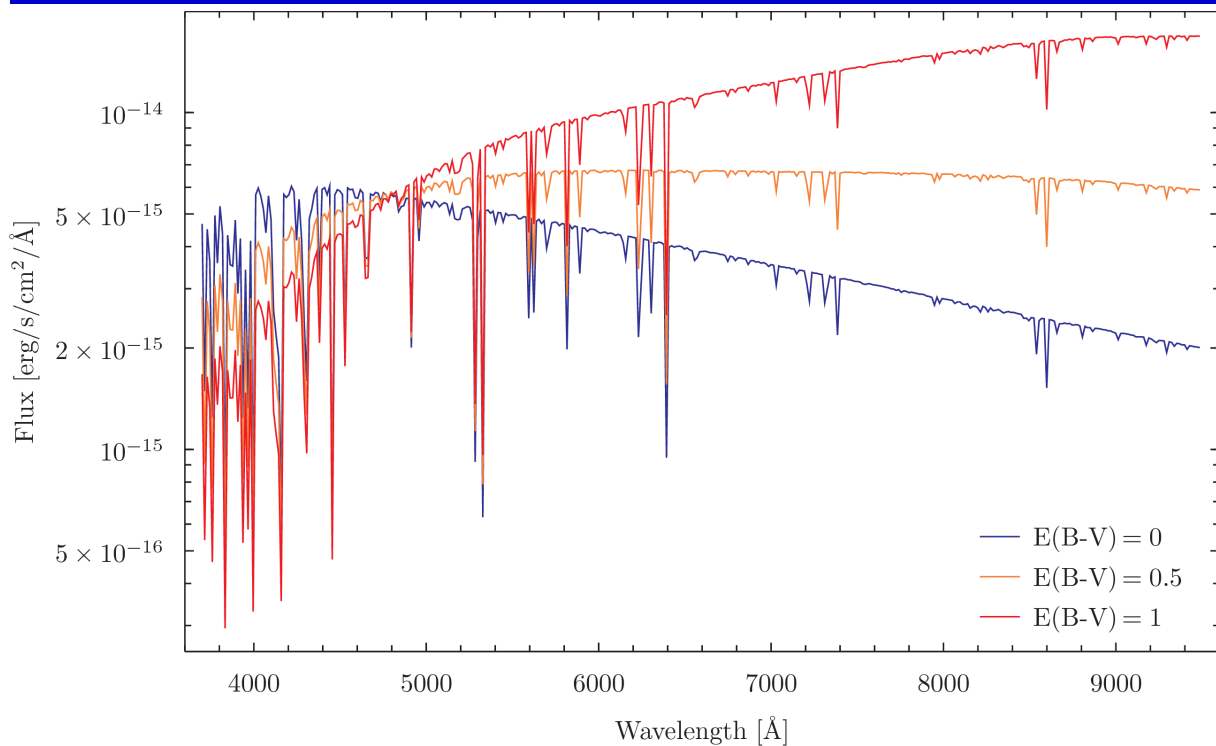


Figure 7-2: The effect of reddening the solar spectrum, holding its observed brightness constant at g=15. To enhance readability, the spectral resolution has been reduced to 250.

In Figure 7-3 we plot the wavelength-dependent SNR of this solar spectrum, for simulated 4MOST observations which achieve an SNR/pixel of 50 in the window 6180 – 6680 Å. This corresponds to the test conditions used in the remainder of this section, where we vary E(B-V) whilst simulating observations each test spectrum with the exposure time required to meet this noise criterion.

It may be observed that while reddening significantly degrades the blue end of the spectrum, the regions red-wards of the 6180 – 6680 Å window achieve a higher SNR in reddened spectra. For elements with lines in the red part of the spectrum, it might be conceivable for the Cannon to perform better with reddened spectra. Conversely, the elements which have their lines predominantly in the blue will see their derived abundances degraded.

In our test framework, the Cannon fits continuum-normalised spectra, and so it does not see the change in the continuum shape. The only effect of reddening on our tests is to increase the noise level in the red end of the spectrum, and decrease the noise level in the blue.



Doc. Title: The IWG7 4MOST Galactic Pipeline (4GP):	
Development Report 3	
Doc no.: MST-TNO-XXX-YYYYY-GGGG-HHHH	
Issue no.: 1.00	Date: 2018-06-11
Document status	Page 17 of 40

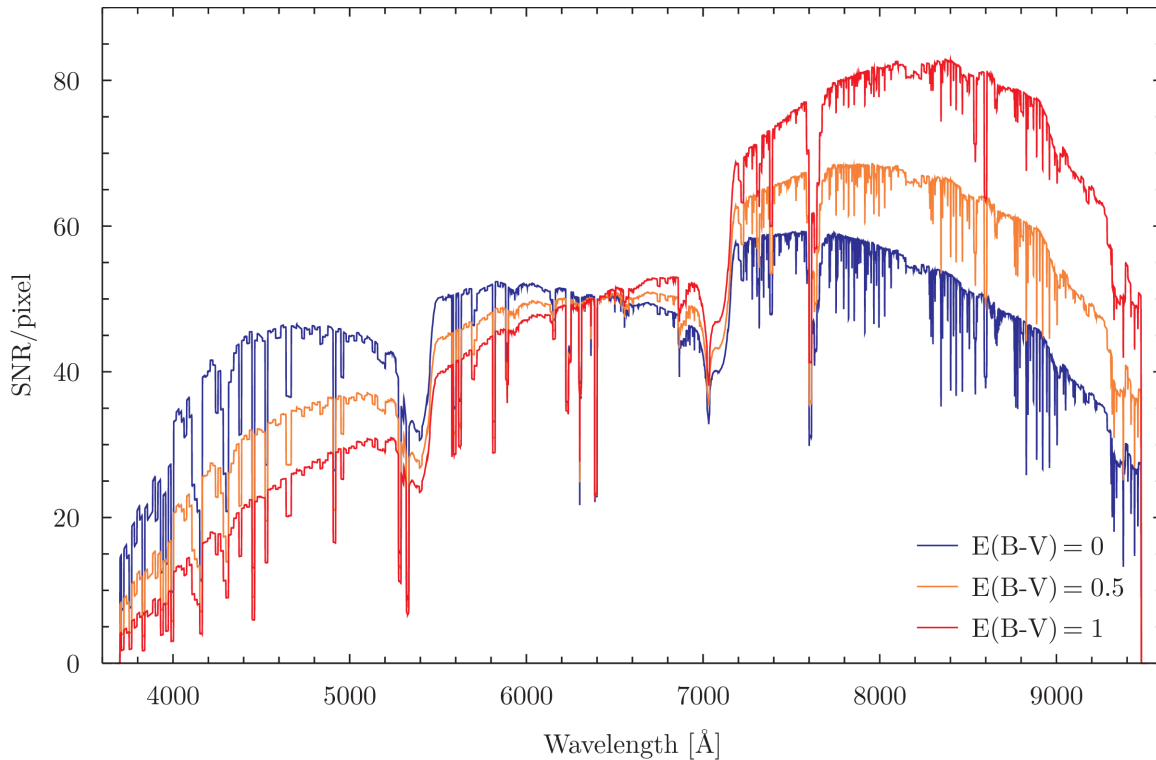


Figure 7-3: The wavelength-dependent signal-to-noise ratio of the solar spectrum, for simulated 4MOST exposures achieving an SNR/pixel of 50 in the window 6180 – 6680 Å.

In Figure 7-4 we plot the RMS offsets in the Cannon's determination of each stellar parameter and abundance as a function of $E(B-V)$, for spectra with an SNR/pixel of 50 in the window 6180 – 6680 Å. We note that the Cannon is very robust against reddening for the range of $E(B-V)$ values expected within the 4MOST surveys. This result holds for both 4MOST LRS and HRS.



Doc. Title: The IWG7 4MOST Galactic Pipeline (4GP):	
Development Report 3	
Doc no.: MST-TNO-XXX-YYYYY-GGGG-HHHH	
Issue no.: 1.00	Date: 2018-06-11
Document status	Page 18 of 40

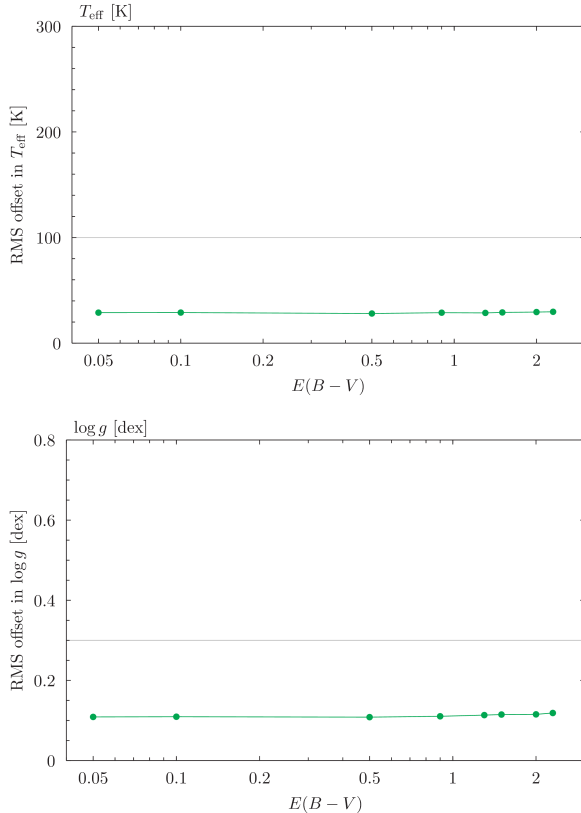
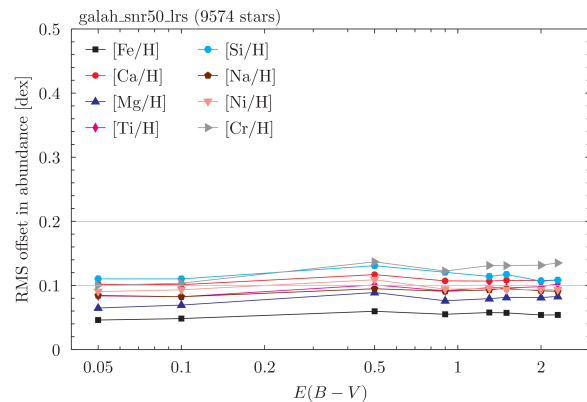
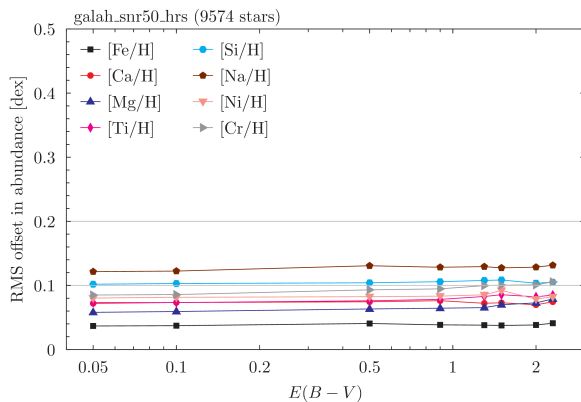
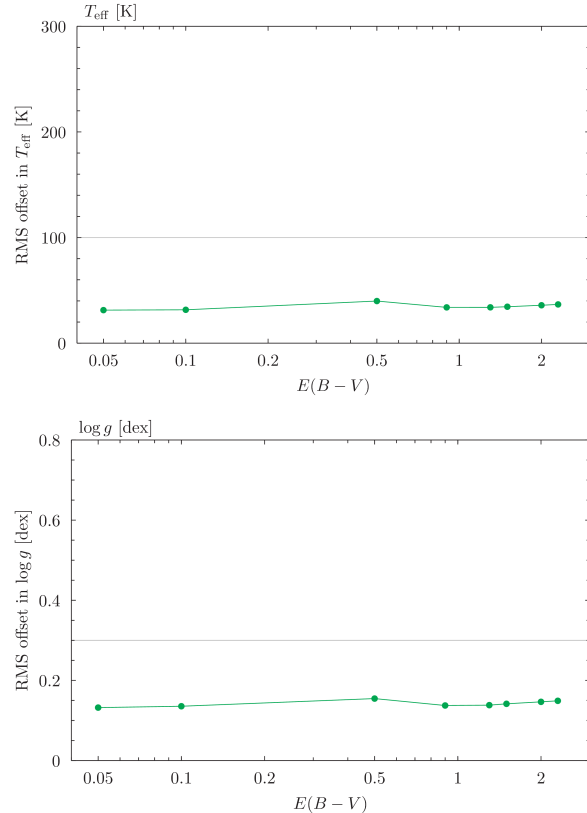
HRS**LRS**

Figure 7-4: The RMS offset in each parameter as a function of $E(B-V)$, for synthetic observations with SNR/pixel=50.



Doc. Title: The IWG7 4MOST Galactic Pipeline (4GP): Development Report 3	
Doc no.: MST-TNO-XXX-YYYYY-GGGG-HHHH	
Issue no.: 1.00	Date: 2018-06-11
Document status	Page 19 of 40

8 Robustness against residual radial velocities

In this section we test the robustness of the Cannon to fitting spectra with residual radial velocities (RVs) which have not been perfectly corrected prior to fitting. The training spectra remain unchanged, while we apply RVs to the test spectra.

This is done by changing the wavelength column of the high-resolution synthetic spectra generated by Turbospectrum, prior to simulating observations of them with 4FS. The code used to do this is the `apply_radial_velocity(v)` method of the `Spectrum` class in 4GP:

https://github.com/dcf21/4most-4gp/blob/20541c6c22f08c24ee0b984b34d66acf03f3a529/src/pythonModules/fourgp_speclib/fourgp_speclib/spectrum.py#L362

For each point in Figure 8-1, we apply a constant RV to the entire test sample of 9,574 stars, and plot the RMS offset in the Cannon's estimates of each stellar parameter and abundance.

The analysis of HRS spectra is not significantly affected for residual RVs less than 2 km/s, while the analysis of LRS spectra can tolerate residual RVs of 10 km/s. These values are well outside the target precision for the determination of the RVs of 4MOST targets.

We have verified that the results do not change for higher SNR or metal-poor stars.



Doc. Title: The IWG7 4MOST Galactic Pipeline (4GP):	
Development Report 3	
Doc no.: MST-TNO-XXX-YYYYY-GGGG-HHHH	
Issue no.: 1.00	Date: 2018-06-11
Document status	Page 20 of 40

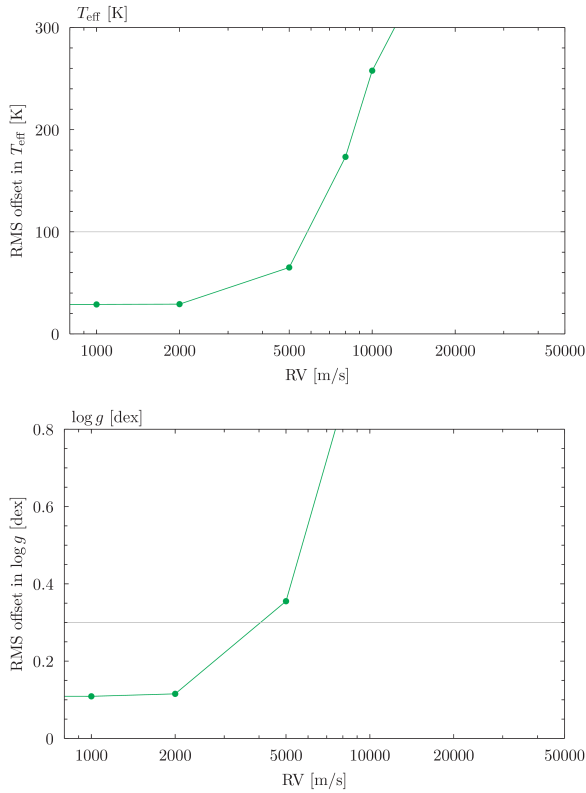
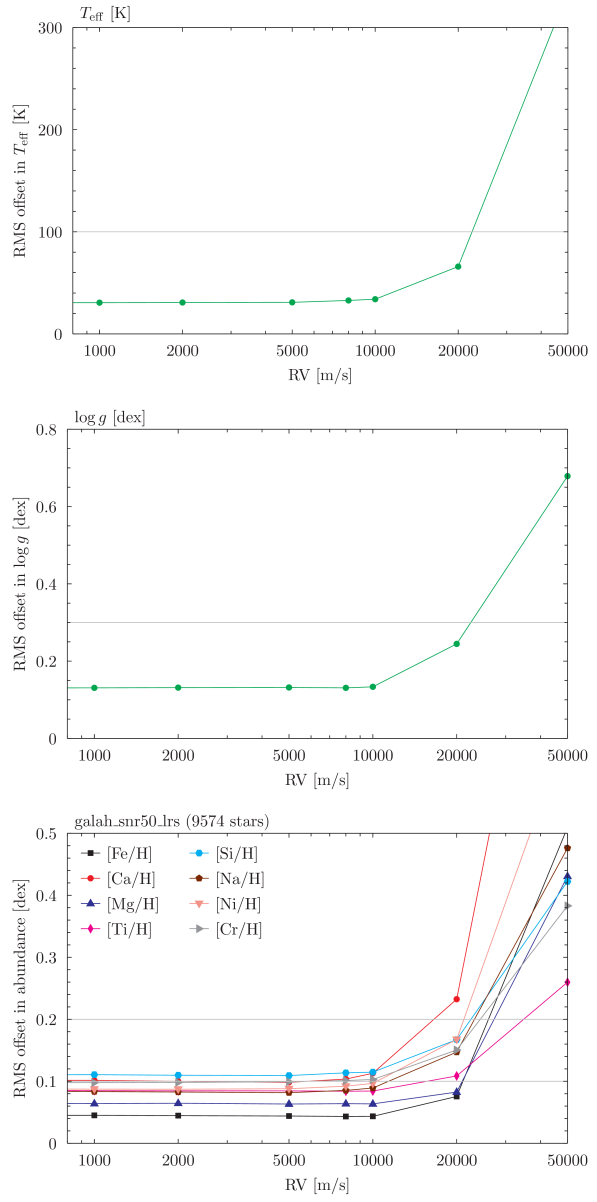
HRS**LRS**

Figure 8-1: The RMS offset in each parameter when uncorrected radial velocities are introduced into the test spectra, for synthetic observations with SNR/pixel=50.



Doc. Title: The IWG7 4MOST Galactic Pipeline (4GP):	
Development Report 3	
Doc no.: MST-TNO-XXX-YYYYY-GGGG-HHHH	
Issue no.: 1.00	Date: 2018-06-11
Document status	Page 21 of 40

9 Robustness against sky contamination

In this section we test the robustness of the Cannon to fitting spectra with some stray light, either from a poorly corrected sky background, or from other stars. Thus far we have only considered pollution with the Sun’s spectrum, however.

In these tests, the training sample remains unchanged, but the test sample is polluted with some fraction of the Sun’s spectrum, which we quantify by the integrated flux across the spectrum coming from the astronomical source versus the polluting source. We test pollution fractions of 0.0001%, 1%, 2% and 5%. After adding this stray light into the high-resolution output of Turbospectrum, we simulate 4MOST HRS observations which achieve a median SNR/pixel of 50 in the window 6180 – 6680 Å.

Figure 9-1 presents the offsets in the Cannon’s determination of T_{eff} and $\log(g)$ for each pollution fraction, mapped across the Kiel diagram. All the panels in this figure denote the offset in T_{eff} by the size of the points, while the offset in $\log(g)$ is represented by their colour. The position of each point on the T_{eff} and $\log(g)$ axes are the star’s *true* stellar parameters, as used to synthesise the spectra, rather than the Cannon’s estimates.

The top-left panel shows the absolute offset between the parameters used to synthesise the spectra, and the Cannon’s estimates with a pollution fraction of 0.0001%. These offsets are almost entirely due to the intrinsic inaccuracy of the Cannon in the absence of contamination. The remaining panels present the additional offsets, each relative to the previous panel, as the pollution fraction is increased to 1%, 2% and finally 5%.

We conclude that sky contamination of up to 2% is not a problem. However, contamination of 5% does appreciably affect our results. The biggest differences are visible at the edges of the parameter space – hot dwarfs and cool giants.

Figure 9-2 presents the offsets in the Cannon’s estimates of [Fe/H] for each contamination fraction. As in the previous figure, we present the results for each contamination level relative to the previous level. The value of [Fe/H] used to synthesise each spectrum is represented by the colour of each point, while the offset in the Cannon’s estimates of [Fe/H] is represented by the size of the points. As before, we conclude that sky contamination of up to 2% is not a problem, but 5% contamination does affect our results.

Figure 9-3 presents the mean offsets in the Cannon’s determination of each of the elemental abundances in our 10-parameter fits. Once again, each panel shows the additional offsets relative to the previous panel. Once again, minimal difference is visible for contamination fractions of up to 2%. A 5% contamination fraction introduces offsets of order 0.02 dex, which is still lower than the accuracy requested by the surveys.



Doc. Title: The IWG7 4MOST Galactic Pipeline (4GP):	
Development Report 3	
Doc no.: MST-TNO-XXX-YYYYY-GGGG-HHHH	
Issue no.: 1.00	Date: 2018-06-11
Document status	Page 22 of 40

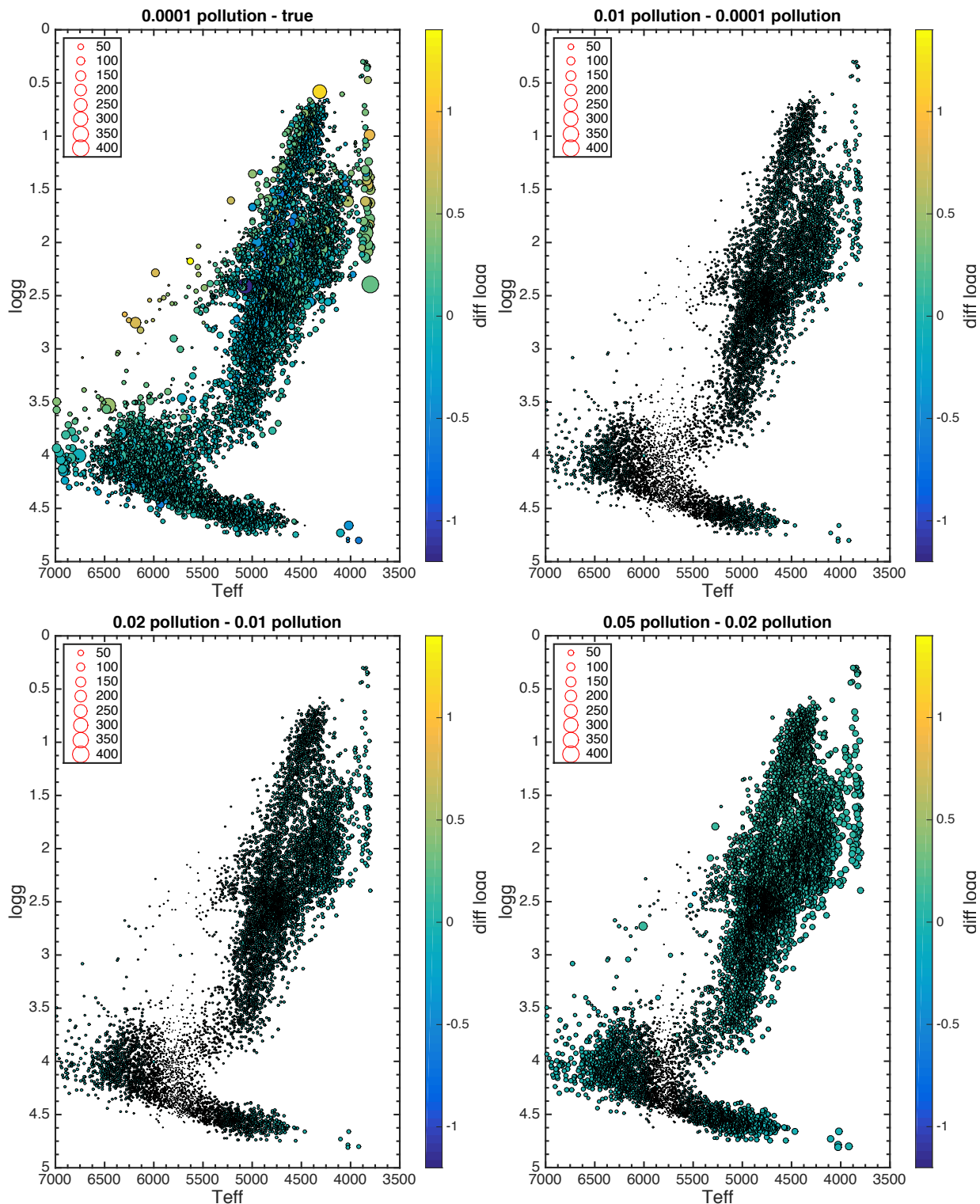


Figure 9-1: Kiel diagrams mapping of offsets in the Cannon's determinations of T_{eff} and $\log(g)$. The colour of each point shows the offset in $\log(g)$; the size of each point shows the offset in T_{eff} . See the text for full details.



Doc. Title: The IWG7 4MOST Galactic Pipeline (4GP):	
Development Report 3	
Doc no.: MST-TNO-XXX-YYYYY-GGGG-HHHH	
Issue no.: 1.00	Date: 2018-06-11
Document status	Page 23 of 40

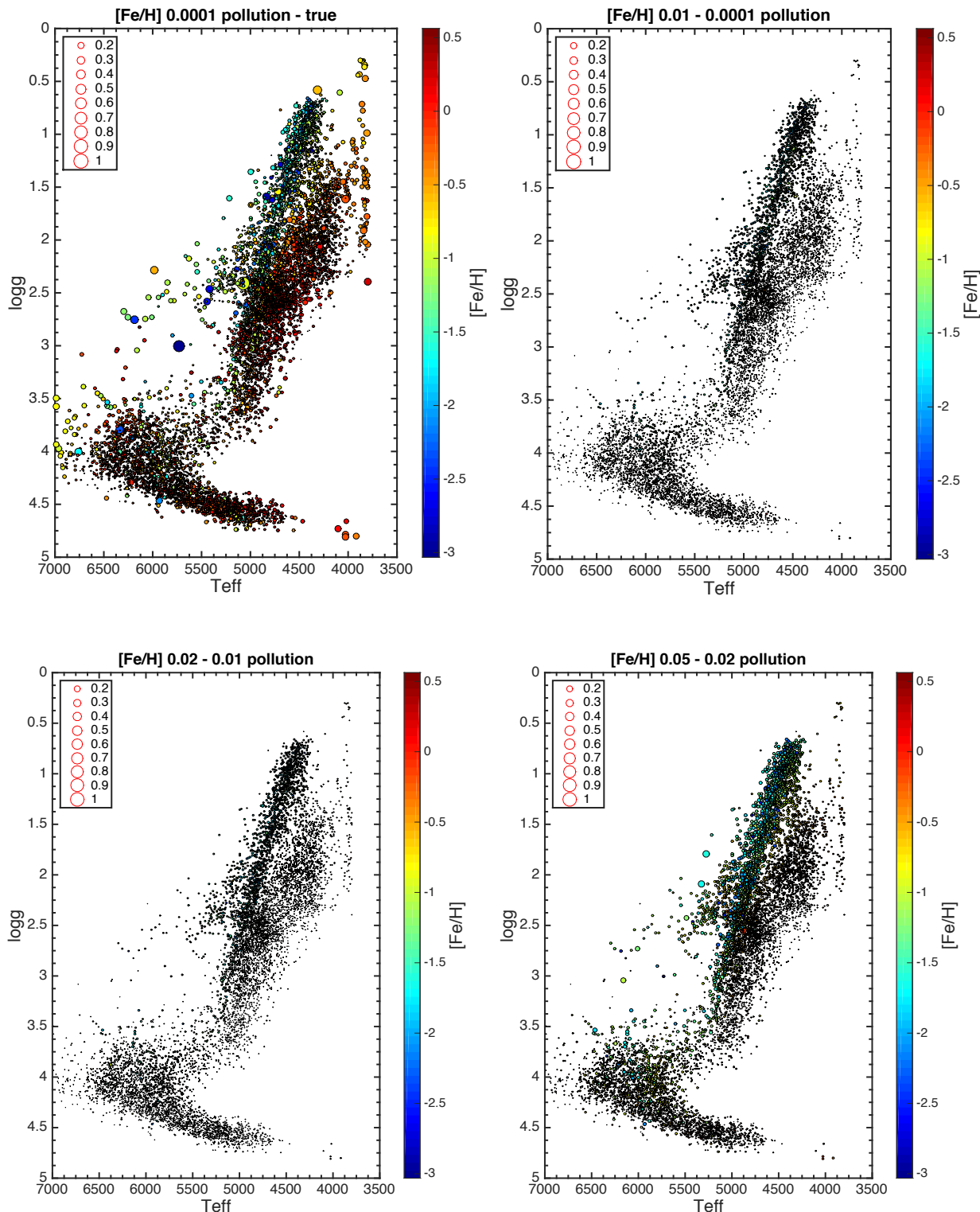


Figure 9-2: Kiel diagrams mapping of offsets in the Cannon's determinations of [Fe/H]. The colour of each point shows the input value of [Fe/H] used to synthesise each spectrum; the size of each point shows the offset in the Cannon's determination of [Fe/H]. See the text for full details.



Doc. Title: The IWG7 4MOST Galactic Pipeline (4GP):	
Development Report 3	
Doc no.: MST-TNO-XXX-YYYYY-GGGG-HHHH	
Issue no.: 1.00	Date: 2018-06-11
Document status	Page 24 of 40

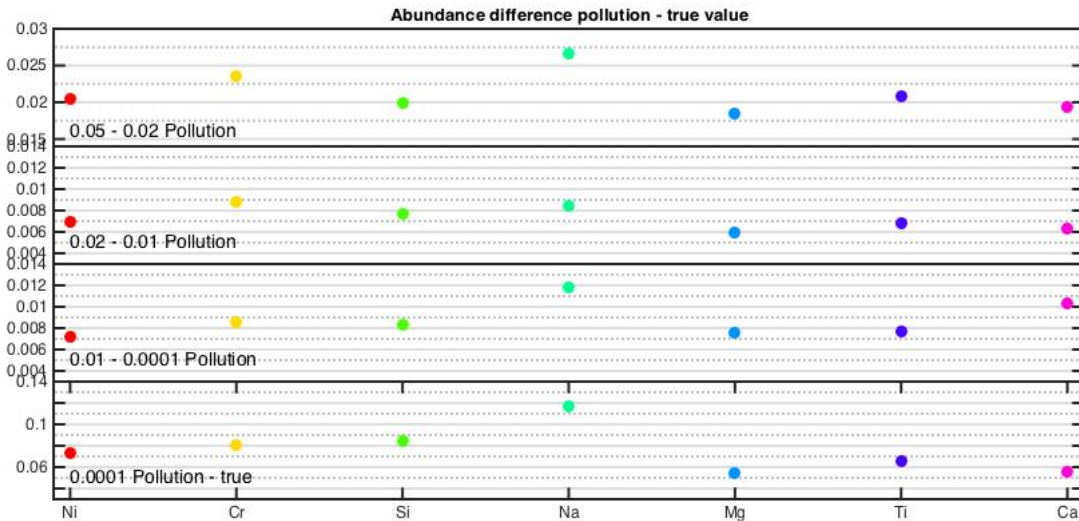


Figure 9-3: Offsets in the Cannon's determinations of the abundances of individual elements.

10 Conclusions and perspectives

The tests conducted so far have been on a handful of elements (Fe, Ca, Mg, Ti, Si, Na, Ni, Cr), however they are more thorough than the ones shown in the previous report and start to implement deviations from training spectra closer to what we expect to be the case when 4MOST will be on the sky.

The current implementation of the Cannon for 4GP is robust to RV shifts up to 2 km/s in HRS and 10 km/s in LRS, regardless the SNR, the stellar type or the metallicity. These values are well above what can be achieved with simple cross-correlation techniques.

As far as running 4GP on reddened spectra, no significant differences have been noticed up to $E(B-V)=2$, provided the SNR of the spectrum is kept constant in the window 6180-6680 Å. That said, the mask that has been used for the Cannon comprise only few lines at the bluest part of the spectra. Future implementations of the pipeline including elements seen only in the blue (e.g. Ba) will have to repeat the extinction tests to see how the abundances determinations are affected.

Finally, regarding sky contaminations, preliminary tests seem to indicate that pollution lower than 2% leave the parameter determination unaffected. Further tests on LRS must still be performed, but we do not expect to show drastically different results.

Future tests and development regarding the pipeline will include:



Doc. Title: The IWG7 4MOST Galactic Pipeline (4GP): Development Report 3	
Doc no.: MST-TNO-XXX-YYYYY-GGGG-HHHH	
Issue no.: 1.00	Date: 2018-06-11
Document status	Page 25 of 40

- Investigate fiber cross-talk contamination.
- Investigate the effect of non perfectly known line profile
- Investigate the effect to telluric residuals in the test spectra
- Addition of a RV measurement module to 4GP: The implementation of the code of Sergey Koposov is for the moment foreseen.
- Addition of new elements in 4GP.

The latter point might require to change the Cannon in order to run it several steps, as recently done in [RD8]. In this case, the T_{eff} , $\log(g)$, $[\text{Fe}/\text{H}]$ and perhaps a handful of elements (less than what determined for the moment) will be first derived, and then the individual abundances will be obtained one after the other.

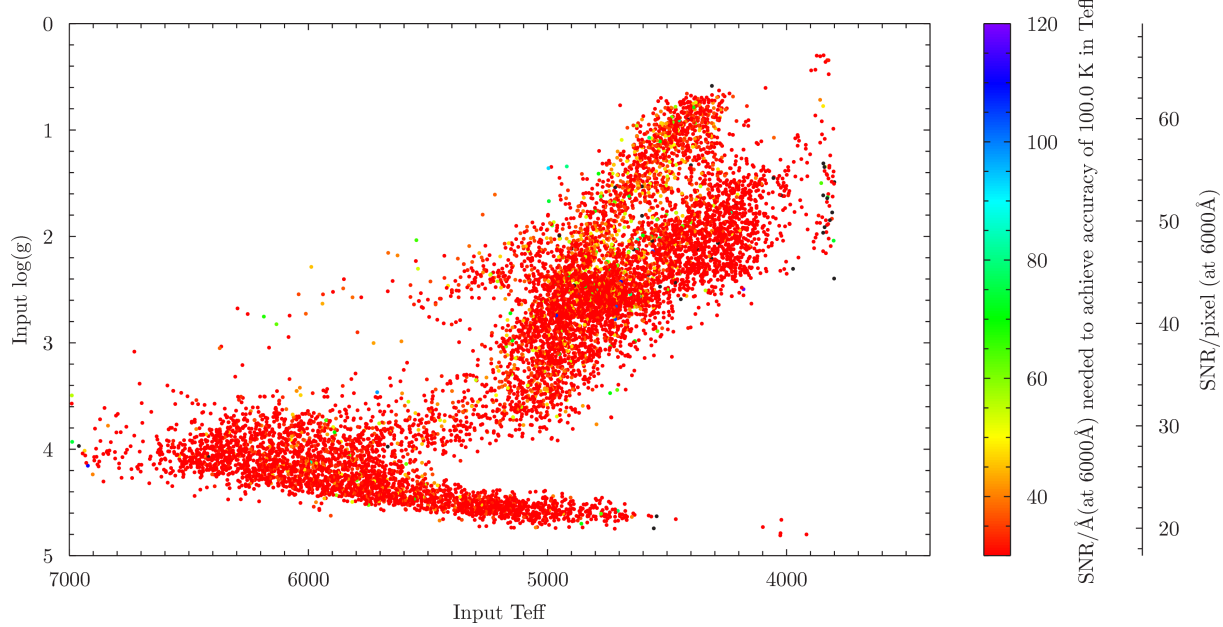


Doc. Title: The IWG7 4MOST Galactic Pipeline (4GP):	
Development Report 3	
Doc no.: MST-TNO-XXX-YYYYY-GGGG-HHHH	
Issue no.: 1.00	Date: 2018-06-11
Document status	Page 26 of 40

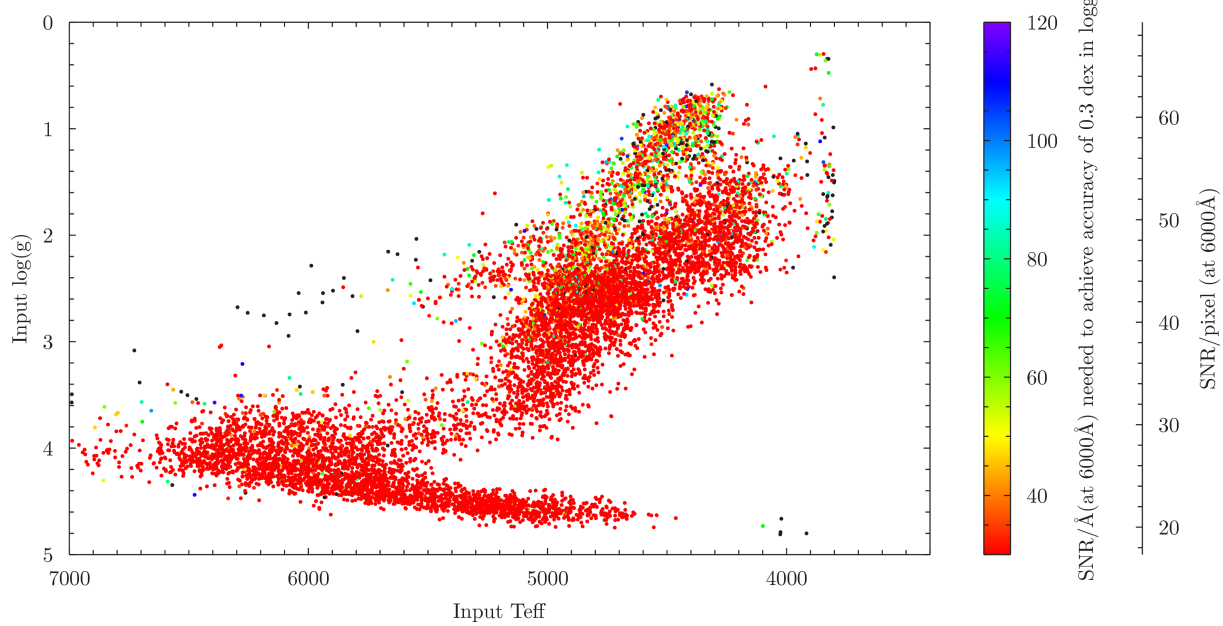
Appendix A: Mapping performance across the HR diagram (LRS)

See Section 6 for more information.

A. 1 T_{eff}

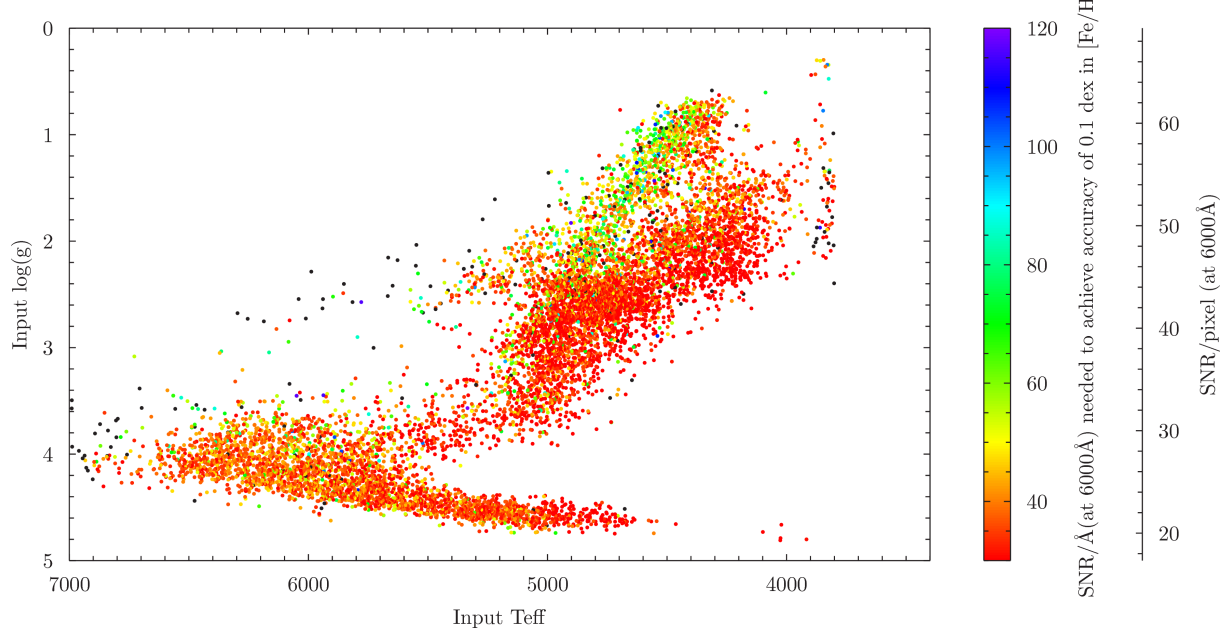
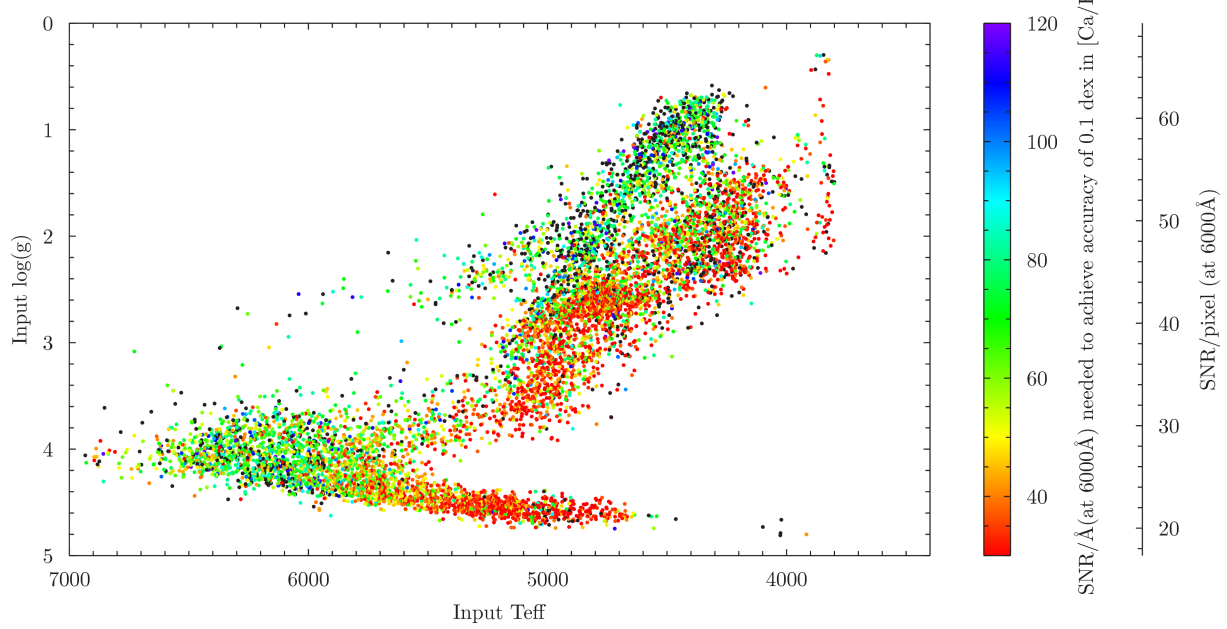


A. 2 $\log(g)$



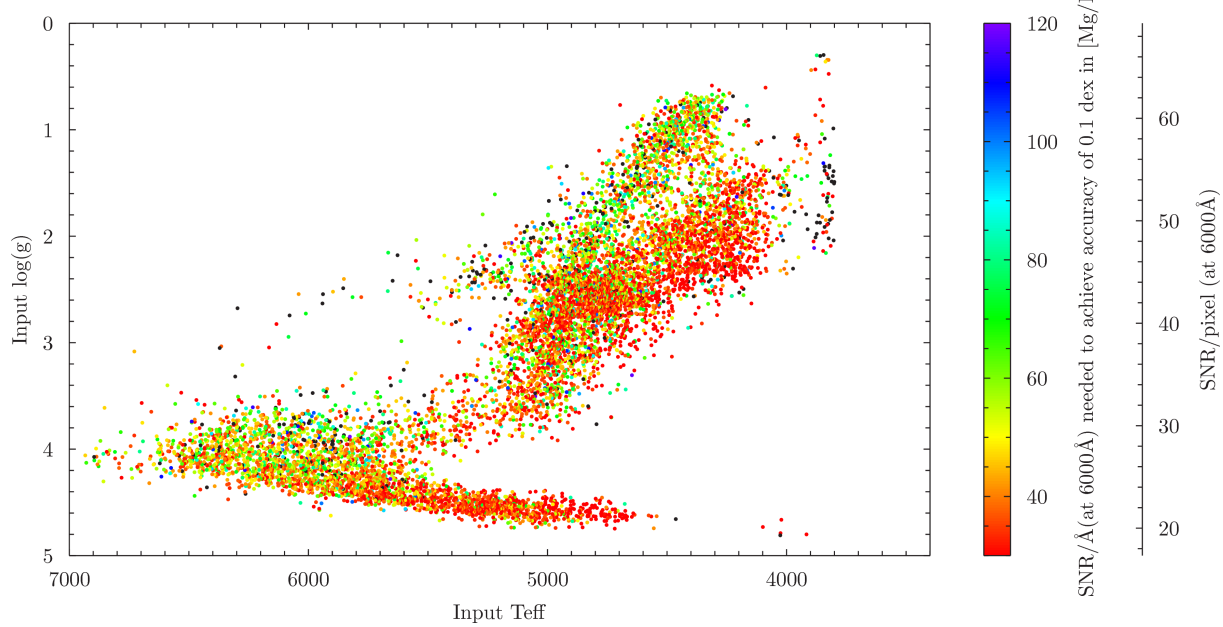
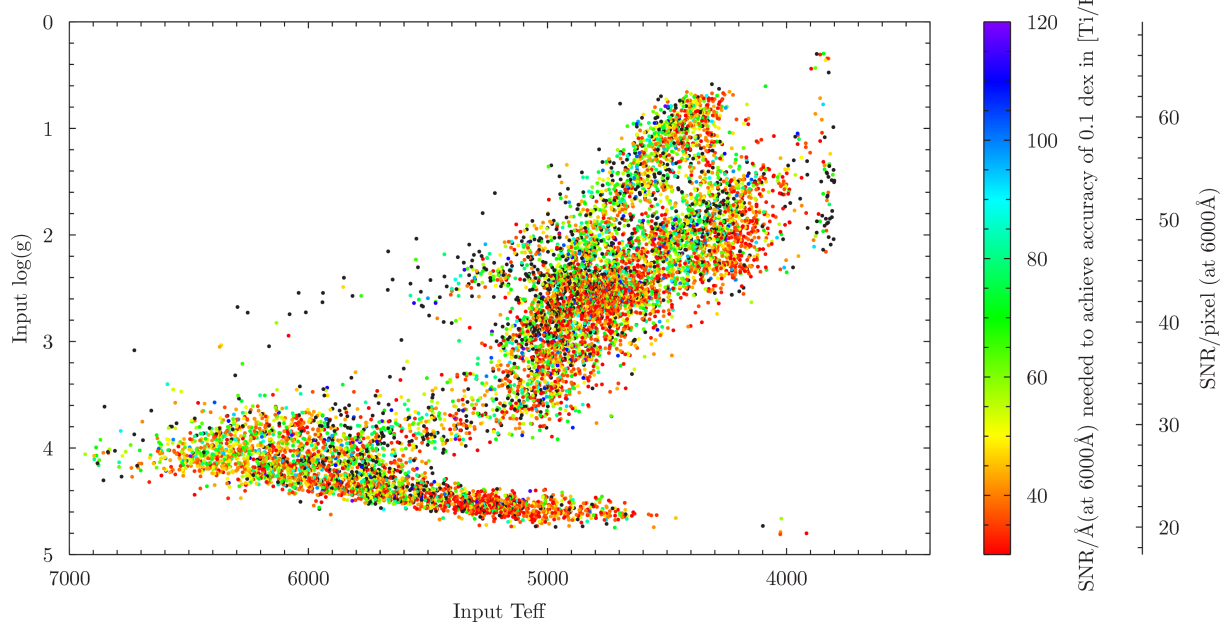


Doc. Title: The IWG7 4MOST Galactic Pipeline (4GP):	
Development Report 3	
Doc no.: MST-TNO-XXX-YYYYY-GGGG-HHHH	
Issue no.: 1.00	Date: 2018-06-11
Document status	Page 27 of 40

A. 3**[Fe/H]****A. 4****[Ca/H]**

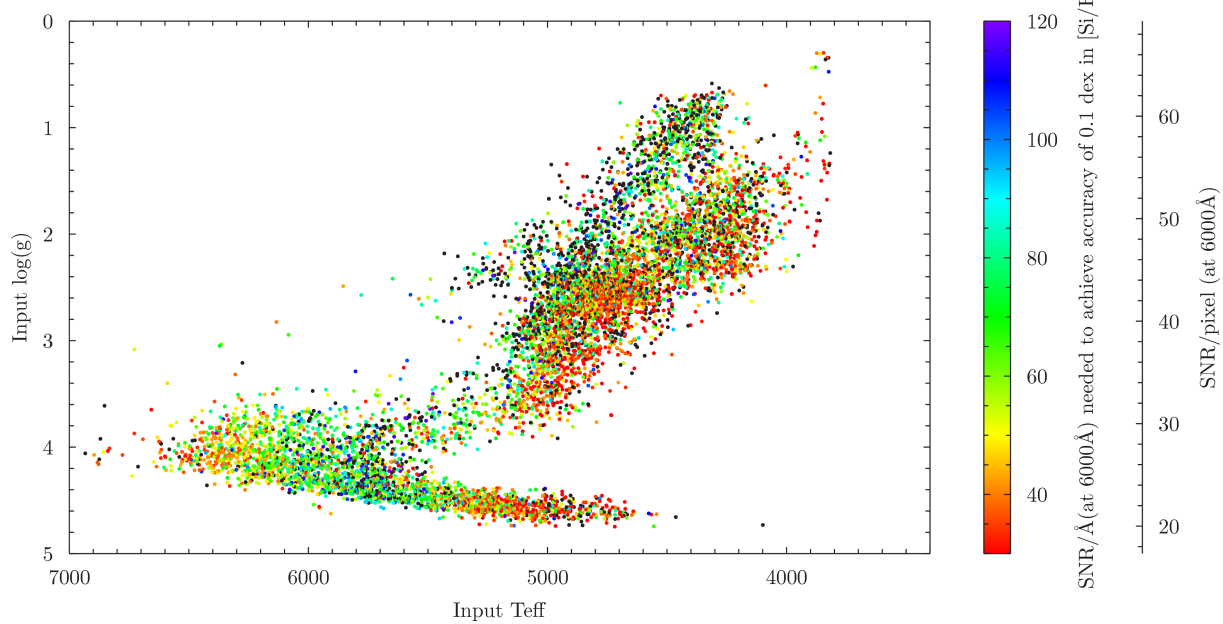
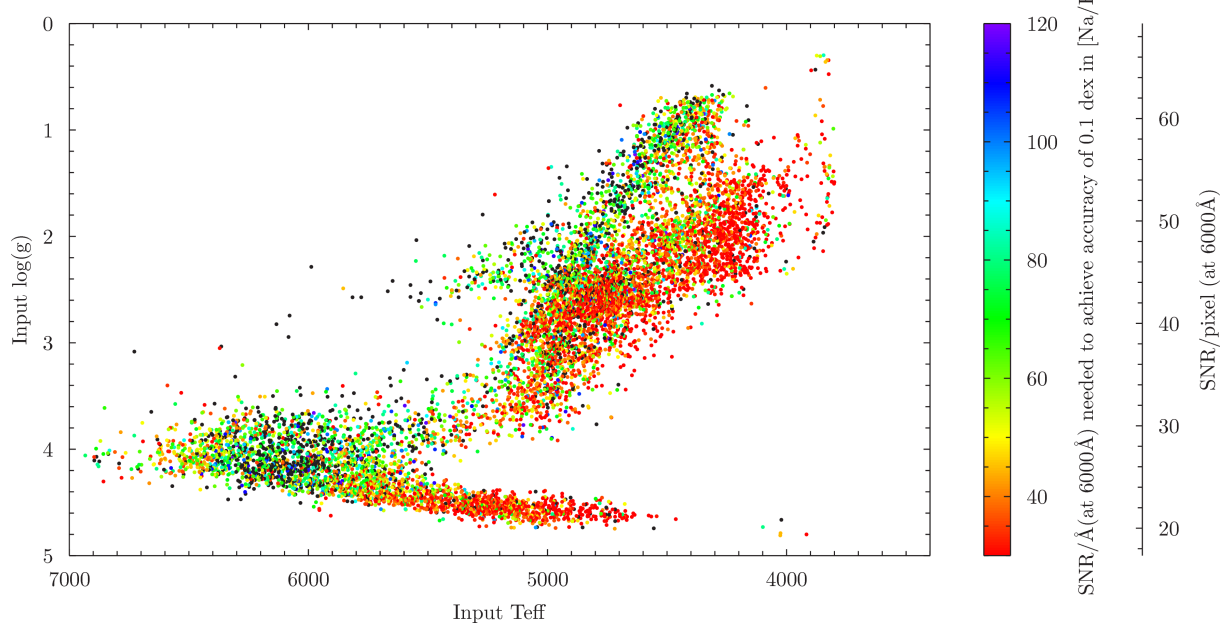


Doc. Title: The IWG7 4MOST Galactic Pipeline (4GP):	
Development Report 3	
Doc no.: MST-TNO-XXX-YYYYY-GGGG-HHHH	
Issue no.: 1.00	Date: 2018-06-11
Document status	Page 28 of 40

A. 5**[Mg/H]****A. 6****[Ti/H]**

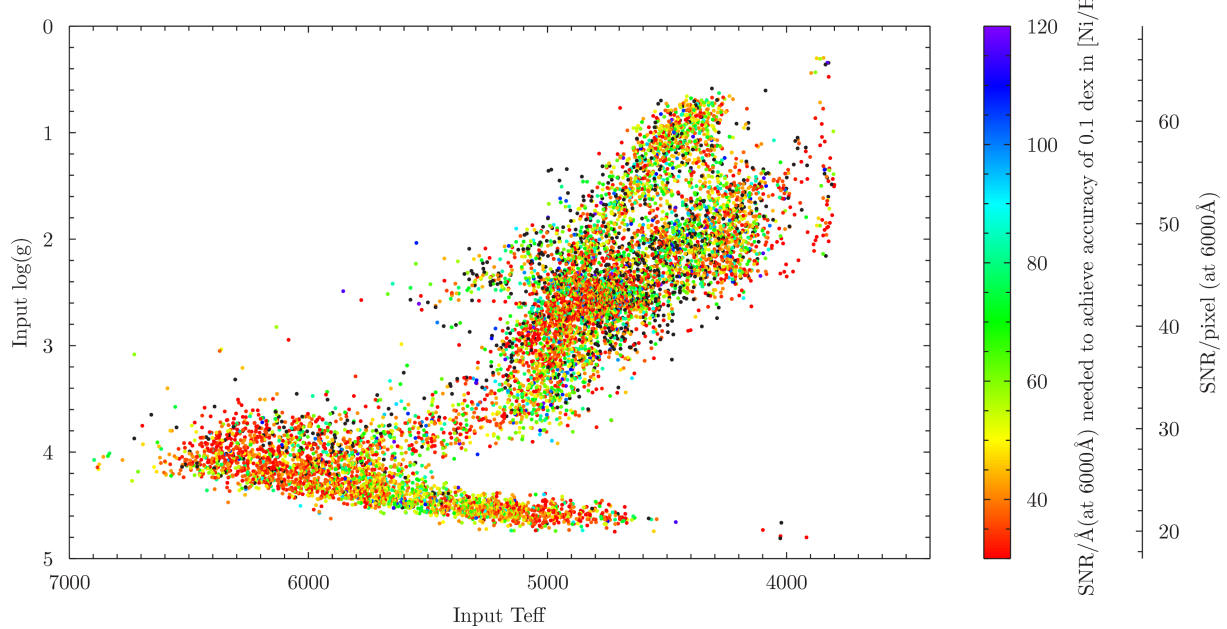
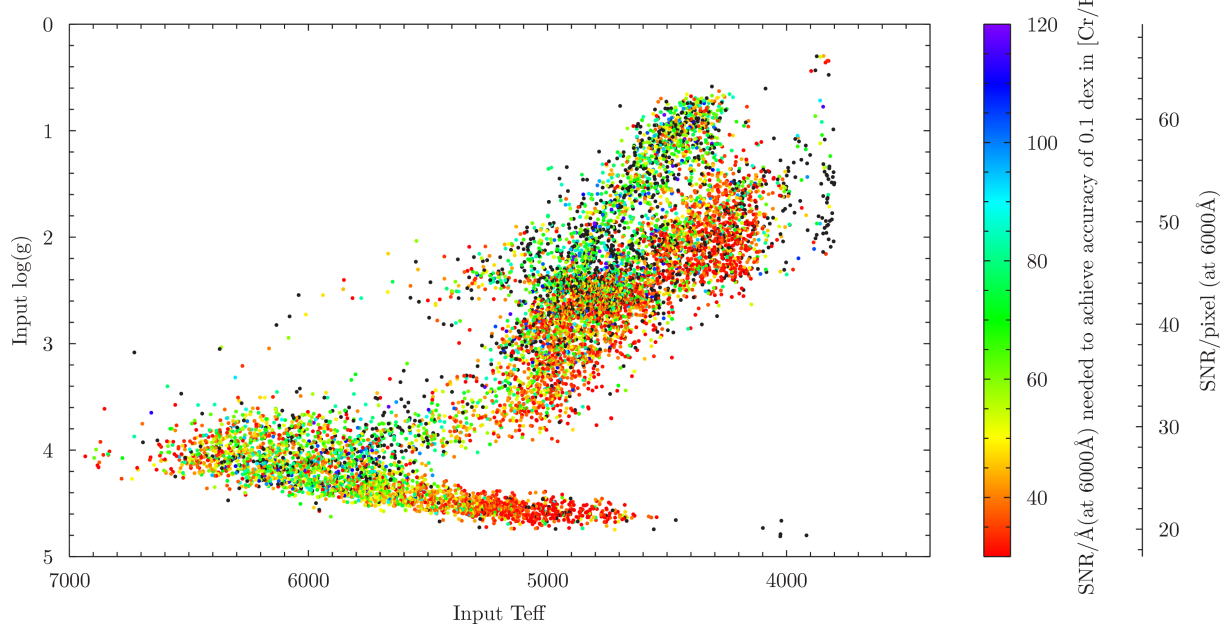


Doc. Title: The IWG7 4MOST Galactic Pipeline (4GP):	
Development Report 3	
Doc no.: MST-TNO-XXX-YYYYY-GGGG-HHHH	
Issue no.: 1.00	Date: 2018-06-11
Document status	Page 29 of 40

A. 7**[Si/H]****A. 8****[Na/H]**



Doc. Title: The IWG7 4MOST Galactic Pipeline (4GP):	
Development Report 3	
Doc no.: MST-TNO-XXX-YYYYY-GGGG-HHHH	
Issue no.: 1.00	Date: 2018-06-11
Document status	Page 30 of 40

A. 9**[Ni/H]****A. 10****[Cr/H]**

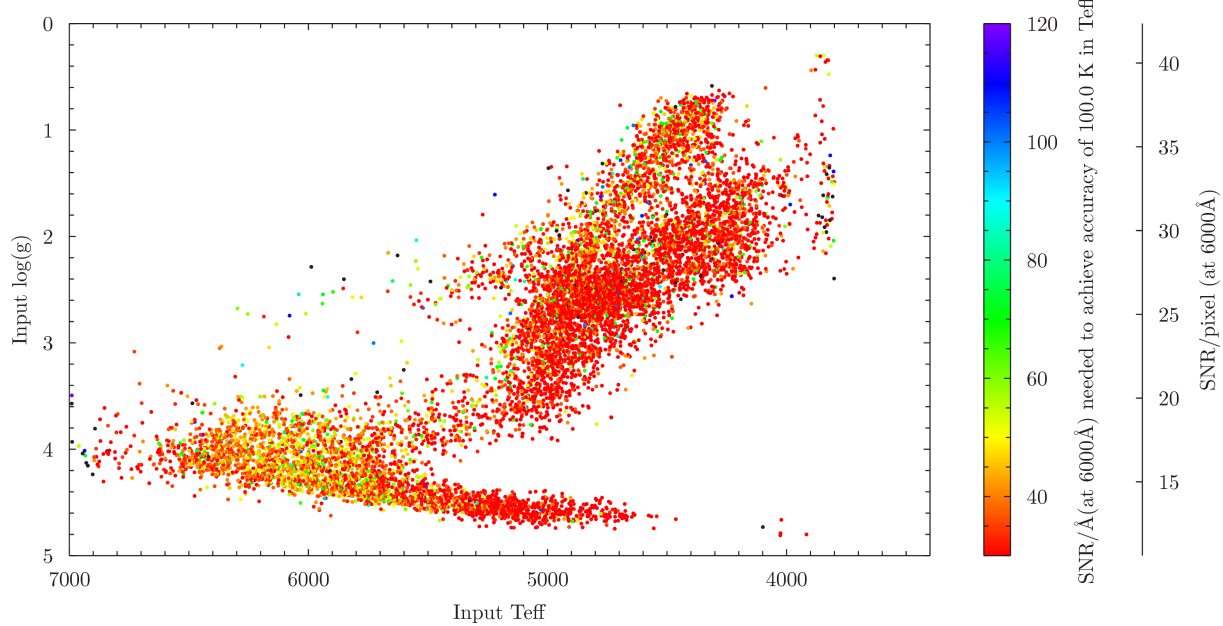


Doc. Title: The IWG7 4MOST Galactic Pipeline (4GP):	
Development Report 3	
Doc no.: MST-TNO-XXX-YYYYY-GGGG-HHHH	
Issue no.: 1.00	Date: 2018-06-11
Document status	Page 31 of 40

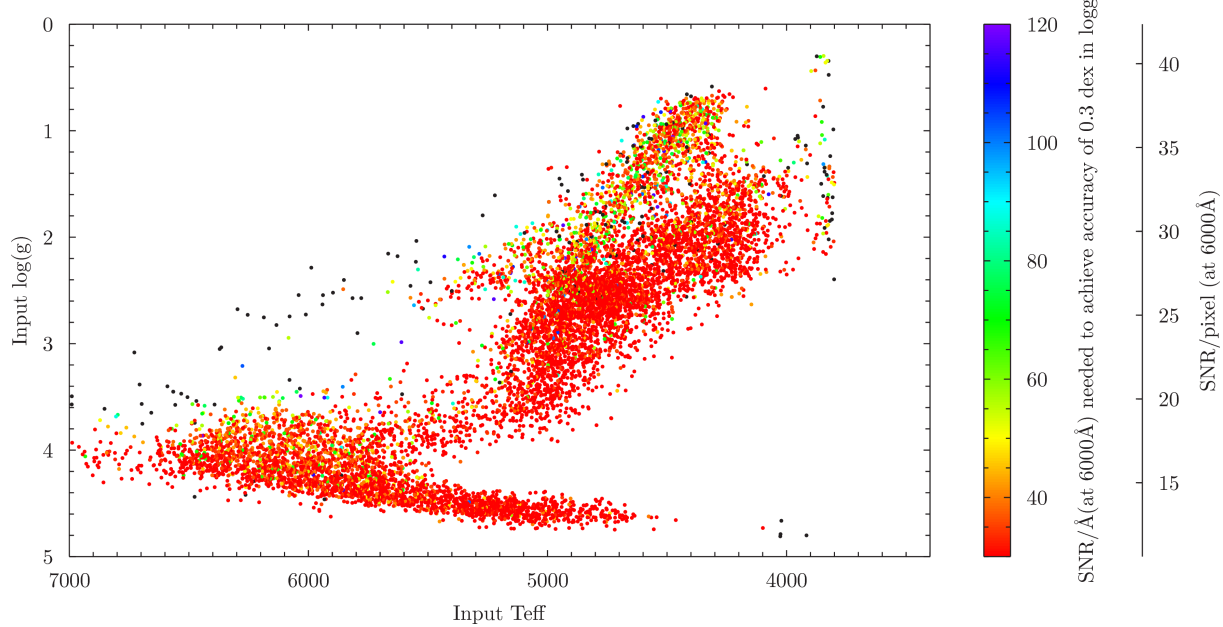
Appendix B: Mapping performance across the HR diagram (HRS)

See Section 6 for more information.

B. 1 T_{eff}

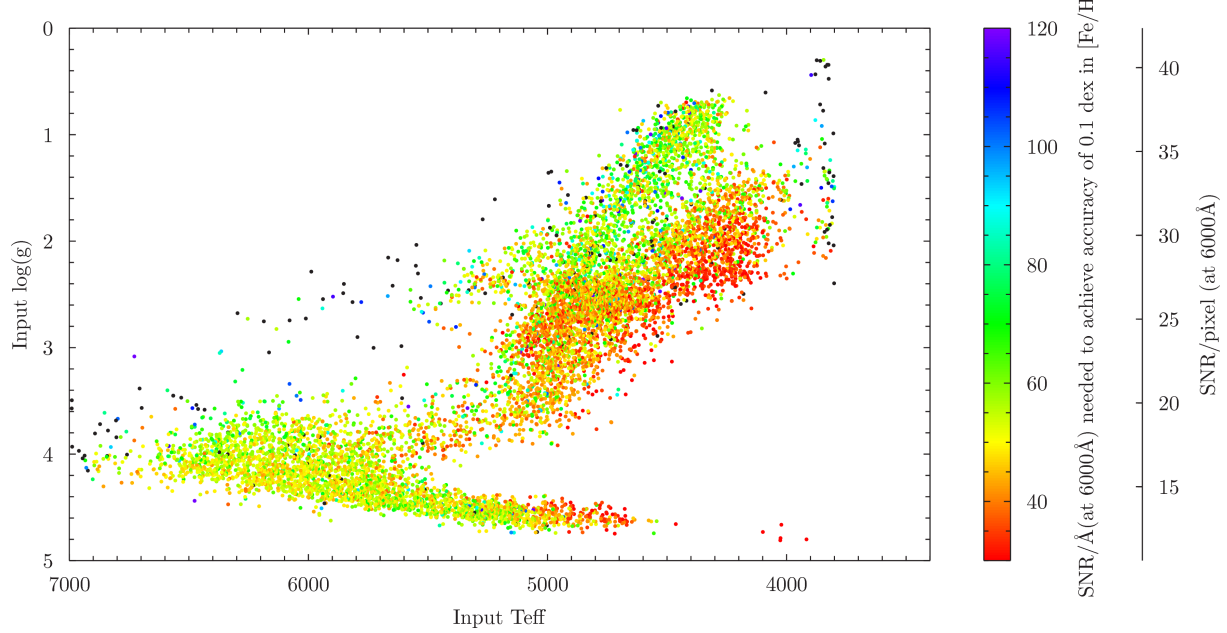
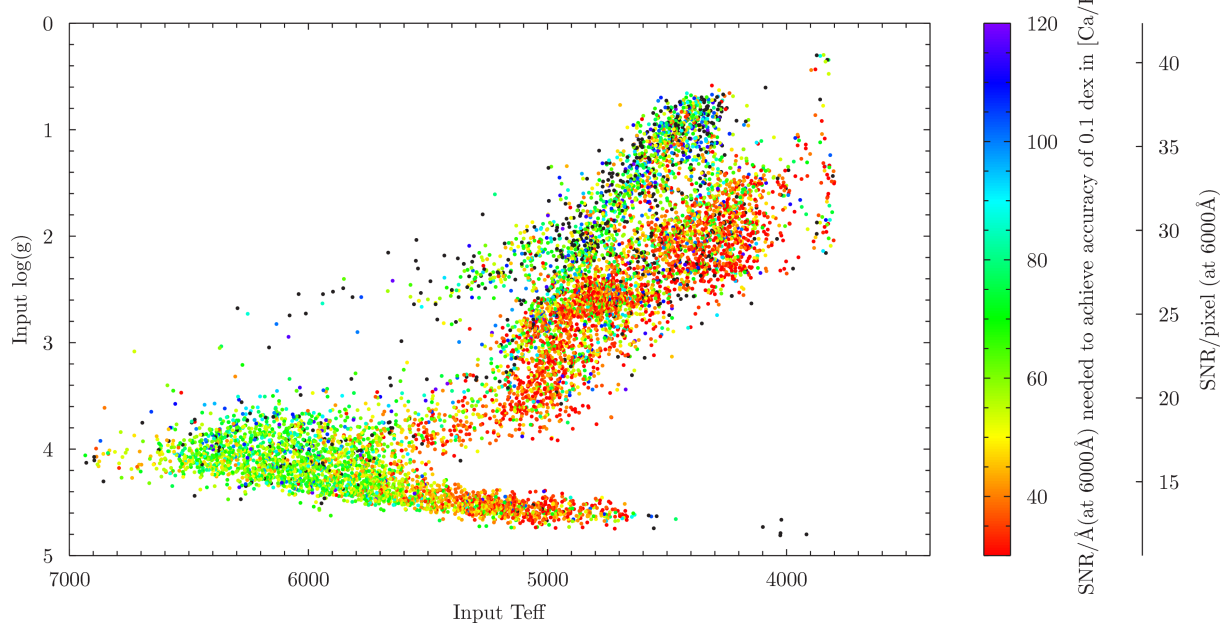


B. 2 $\log(g)$



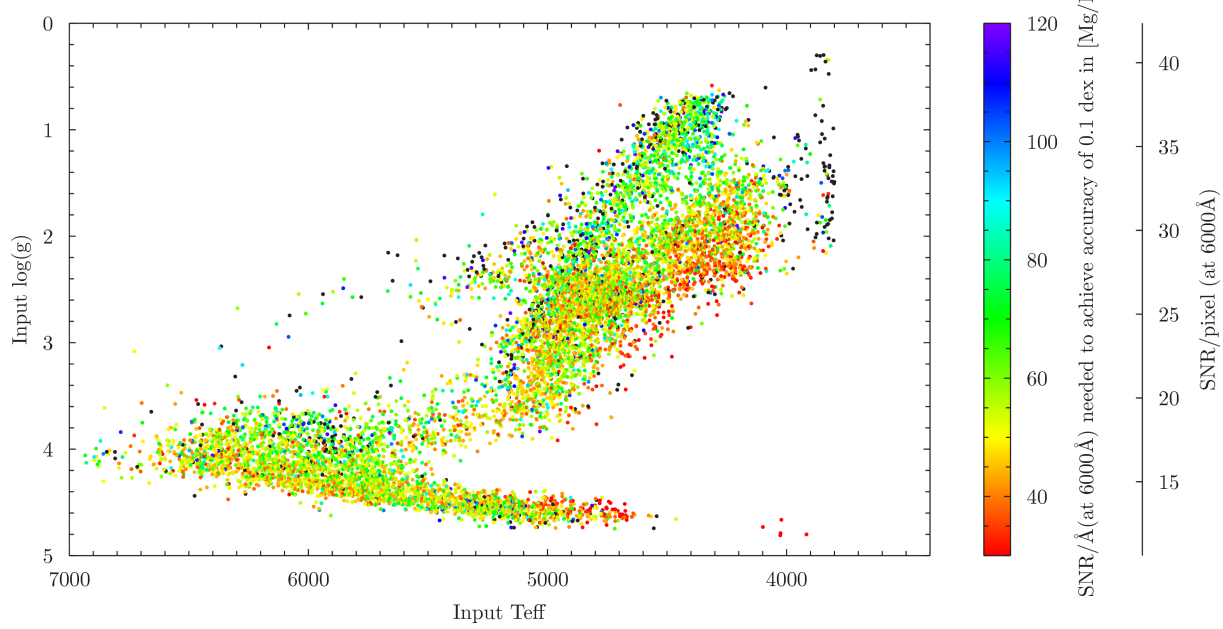
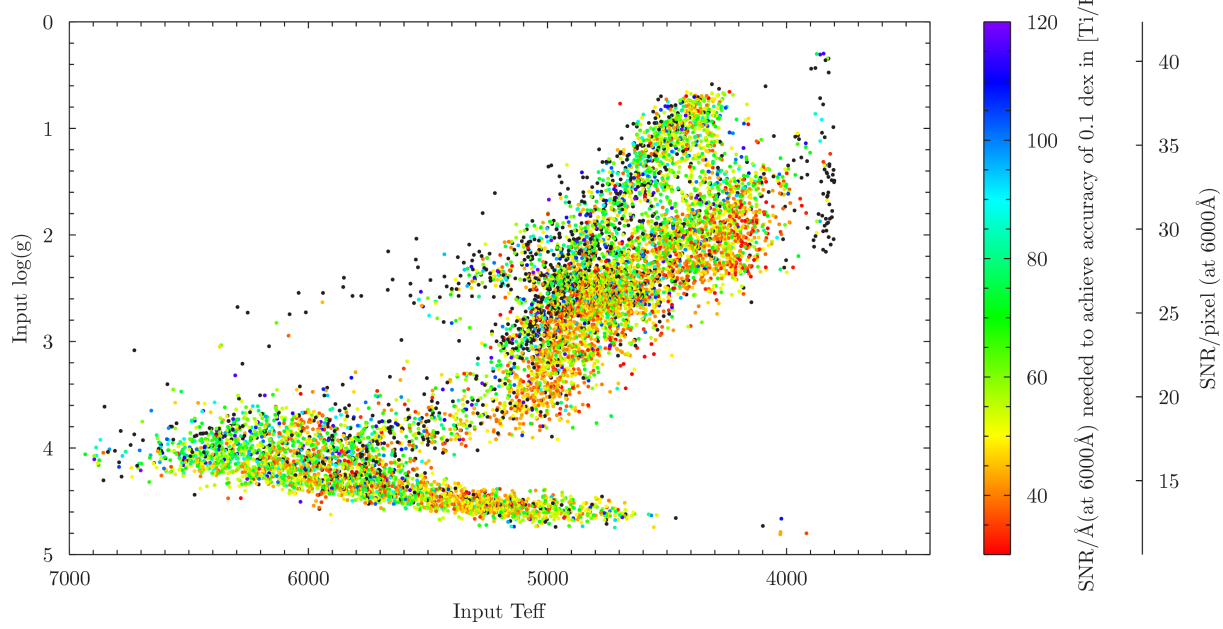


Doc. Title: The IWG7 4MOST Galactic Pipeline (4GP):	
Development Report 3	
Doc no.: MST-TNO-XXX-YYYYY-GGGG-HHHH	
Issue no.: 1.00	Date: 2018-06-11
Document status	Page 32 of 40

B. 3**[Fe/H]****B. 4****[Ca/H]**

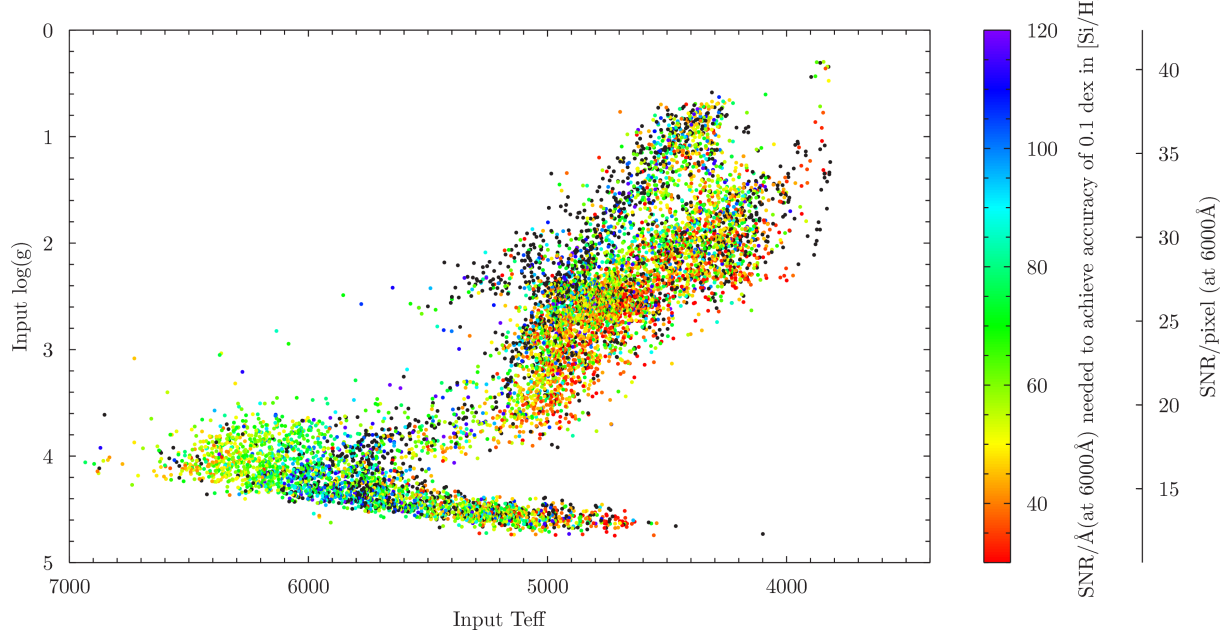
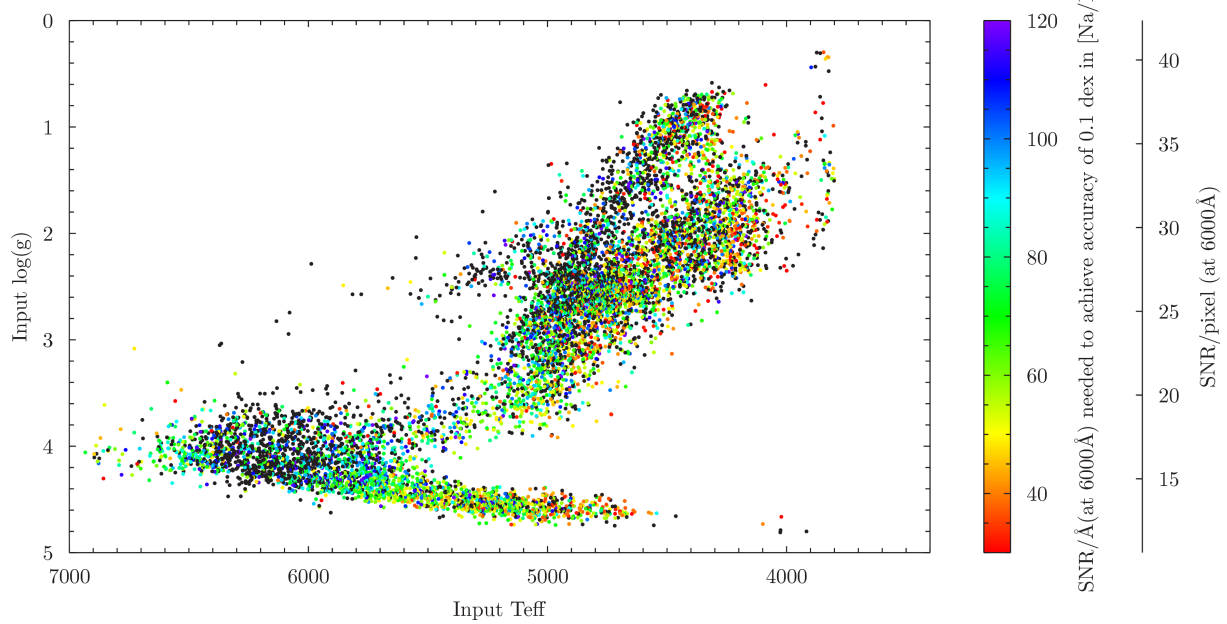


Doc. Title: The IWG7 4MOST Galactic Pipeline (4GP):	
Development Report 3	
Doc no.: MST-TNO-XXX-YYYYY-GGGG-HHHH	
Issue no.: 1.00	Date: 2018-06-11
Document status	Page 33 of 40

B. 5**[Mg/H]****B. 6****[Ti/H]**

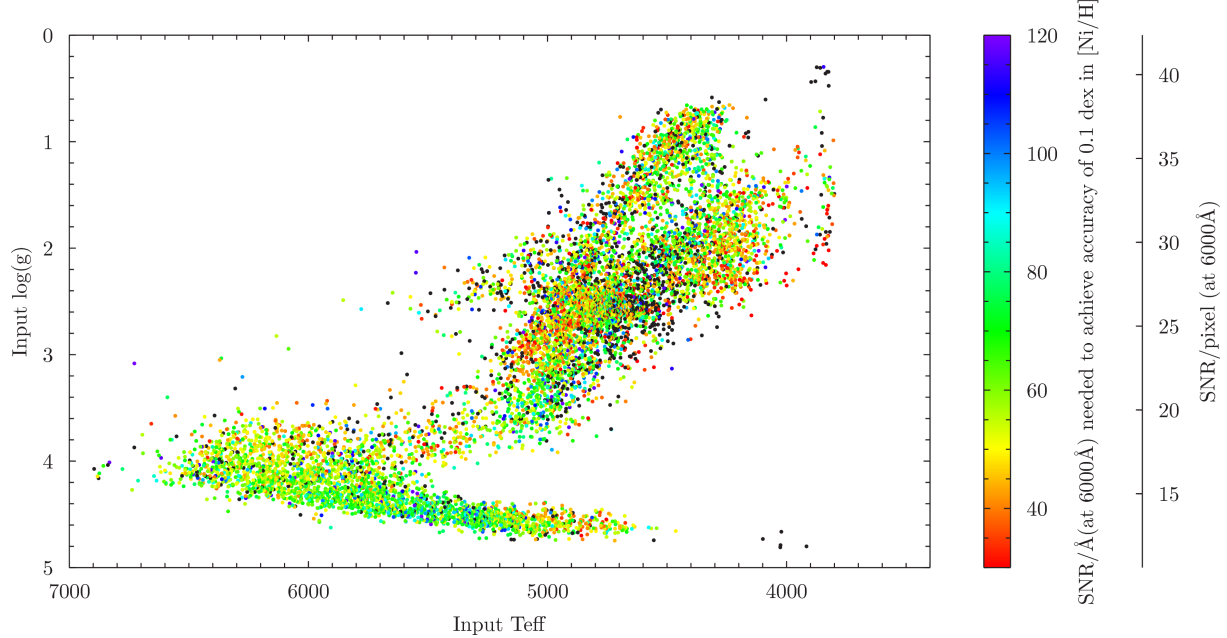
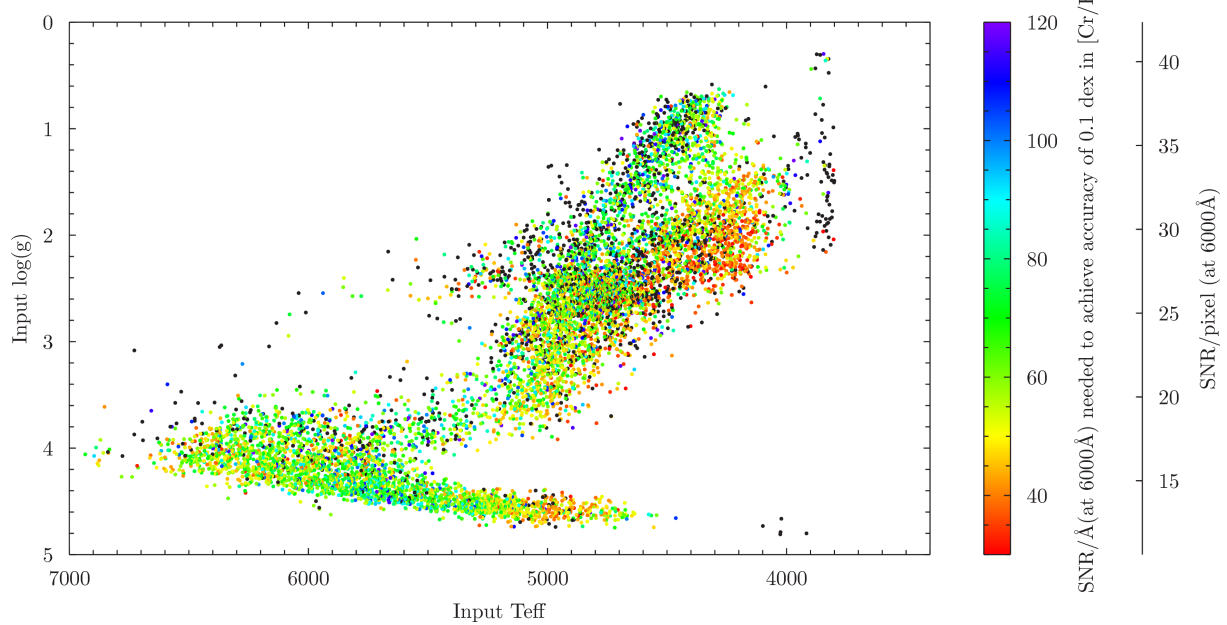


Doc. Title: The IWG7 4MOST Galactic Pipeline (4GP):	
Development Report 3	
Doc no.: MST-TNO-XXX-YYYYY-GGGG-HHHH	
Issue no.: 1.00	Date: 2018-06-11
Document status	Page 34 of 40

B. 7**[Si/H]****B. 8****[Na/H]**



Doc. Title: The IWG7 4MOST Galactic Pipeline (4GP):	
Development Report 3	
Doc no.: MST-TNO-XXX-YYYYY-GGGG-HHHH	
Issue no.: 1.00	Date: 2018-06-11
Document status	Page 35 of 40

B. 9**[Ni/H]****B. 10****[Cr/H]**



Doc. Title: The IWG7 4MOST Galactic Pipeline (4GP): Development Report 3								
Doc no.: MST-TNO-XXX-YYYYY-GGGG-HHHH								
Issue no.: 1.00					Date: 2018-06-11			
Document status					Page 36 of 40			

Appendix C Line list

Species	$\lambda / \text{\AA}$	EP	$\log(g_f)$	w	f_{ef}	f_b	f_s	
H α	6470-6650							
H β	4861.35							
Mg B	5100-5250							
Ca I	6152-6172							
Mg I	5167.3216	2.709	-0.931	2	1	1	3	
Mg I	5172.6843	2.712	-0.450	1	1	1	3	
Mg I	5183.6042	2.717	-0.239	1	1	1	3	
Li I	6707.7635	0.000	-0.002	1	1	1	3	
Li I	6707.9145	0.000	-0.303	1	1	1	3	
C I	5380.3252	7.685	-1.615	1	1	1	1	
C I	6587.6100	8.537	-1.021	1	1	1	1	
O I	6300.3038	0.000	-9.715	2	1	0	2	
O I	6363.7760	0.020	-10.190	2	1	0	2	
O I	7771.9440	9.146	0.369	2	2	1	3	
O I	7774.1660	9.146	0.223	2	2	1	3	
O I	7775.3880	9.146	0.002	2	2	1	3	
Na I	5682.6333	2.102	-0.706	2	2	1	3	
Na I	5688.2050	2.104	-0.404	1	2	1	3	
Na I	5889.9509	0.000	0.108	1	1	1	3	
Na I	5895.9242	0.000	-0.144	1	1	1	3	
Na I	6154.2255	2.102	-1.547	1	2	0	3	
Na I	6160.7471	2.104	-1.246	1	2	0	3	
Mg I	4571.0956	0.000	-5.623	1	2	0	3	
Mg I	4702.9909	4.346	-0.440	1	2	1	3	
Mg I	5528.4047	4.346	-0.498	1	2	1	3	
Mg I	5711.0880	4.346	-1.724	1	2	0	3	
Mg I	6318.7170	5.108	-2.103	2	2	0	3	
Mg I	6319.2370	5.108	-2.324	2	2	0	3	
Mg I	6319.4930	5.108	-2.803	2	2	0	3	
Mg I	7387.6890	5.753	-1.000	1	2	0	3	
Mg I	7691.5500	5.753	-0.783	1	2	0	3	
Al I	6698.6730	3.143	-1.870	1	2	0	1	
Al I	7835.3090	4.022	-0.649	1	3	0	3	
Al I	7836.1340	4.022	-0.494	1	3	0	3	
Si I	5665.5545	4.920	-1.940	2	1	0	3	
Si I	5690.4250	4.930	-1.773	1	1	1	3	
Si I	5793.0726	4.930	-1.963	1	1	1	3	
Si I	5948.5410	5.082	-1.130	1	1	0	3	
Si I	6125.0209	5.614	-1.464	2	3	0	1	
Si I	6131.5729	5.616	-1.556	1	3	0	3	
Si I	6131.8516	5.616	-1.615	2	3	0	3	
Si I	6142.4832	5.619	-1.295	2	3	0	3	
Si I	6145.0159	5.616	-1.310	2	3	0	3	
Si I	6155.1343	5.619	-0.754	1	3	0	3	
Si I	6237.3191	5.614	-0.975	1	3	0	3	
Si I	6243.8146	5.616	-1.242	2	3	0	1	
Si I	6244.4655	5.616	-1.093	2	3	0	1	
Si I	6721.8481	5.863	-1.062	2	2	0	3	
Si I	7034.9006	5.871	-0.880	2	1	0	3	
Si I	7250.6269	5.619	-1.220	2	1	0	3	
Si I	7405.7718	5.614	-0.820	1	1	0	3	
Si I	7423.4964	5.619	-0.176	2	3	0	1	
Si II	7680.2660	5.863	-0.690	1	1	0	3	
Si II	7849.9664	6.191	-0.714	2	3	0	1	
Si II	7918.3840	5.954	-0.610	2	1	0	1	
Si II	7932.3479	5.964	-0.470	1	1	0	3	
Si II	7944.0006	5.984	-0.310	2	1	0	1	
Si II	6347.1087	8.121	0.169	2	1	0	1	
Si II	6371.3714	8.121	-0.044	2	1	0	1	
K I	7698.9643	0.000	-0.154	1	3	1	3	
Ca I	4578.5510	2.520	-0.697	2	1	0	1	
Ca I	5261.7040	2.521	-0.579	2	1	1	3	
Ca I	5512.9800	2.933	-0.464	2	1	0	3	
Ca I	5581.9650	2.523	-0.555	1	1	1	3	
Ca I	5590.1140	2.521	-0.571	2	1	1	3	
Ca I	5601.2770	2.526	-0.523	1	1	1	3	
Ca I	5867.5620	2.933	-1.570	1	1	0	3	
Ca I	6122.2170	1.886	-0.316	1	1	1	3	
Ca I	6161.2970	2.523	-1.266	2	1	1	3	
Ca I	6166.4390	2.521	-1.142	1	1	1	3	
Ca I	6169.0420	2.523	-0.797	1	1	1	3	
Ca I	6169.5630	2.526	-0.478	1	1	1	3	
Ca I	6439.0750	2.526	0.390	1	1	1	3	
Ca I	6455.5980	2.523	-1.290	1	1	1	3	
Ca I	6471.6620	2.526	-0.686	1	1	1	3	
Ca I	6493.7810	2.521	-0.109	1	1	1	3	
Ca I	6499.6500	2.523	-0.818	1	1	1	2	
Sc I	4743.8300	1.448	0.422	2	1	1	2	
Sc I	5484.6260	1.851	0.148	2	1	1	2	
Sc I	5520.4970	1.865	0.293	2	1	0	2	
Sc I	5671.8210	1.448	0.495	1	1	0	2	
Sc I	6210.6580	0.000	-1.529	1	1	1	2	
Sc II	5239.8130	1.455	-0.765	2	1	0	1	
Sc II	5526.7900	1.768	0.024	1	1	0	3	
Sc II	5657.8960	1.507	-0.603	2	1	0	3	
Sc II	5684.2020	1.507	-1.074	2	1	0	3	
Sc II	6279.7530	1.500	-1.252	2	3	0	3	
Sc II	6245.6366	1.507	-1.022	2	3	0	3	
Sc II	6604.6010	1.357	-1.309	1	1	0	3	
Ti I	4512.7344	0.836	-0.400	2	1	1	3	
Ti I	4518.0220	0.826	-0.250	2	1	1	3	
Ti I	4555.4839	0.848	-0.400	2	1	1	3	
Ti I	4617.2688	1.749	0.440	1	1	1	3	
Ti I	4623.0972	1.739	0.160	2	1	1	3	
Ti I	4758.1180	2.249	0.510	2	1	1	3	
Ti I	4759.2696	2.256	0.590	2	1	1	3	
Ti I	4820.4110	1.503	-0.380	1	1	1	3	
Ti I	4913.6136	1.873	0.220	2	1	1	3	
Ti I	4981.7304	0.848	0.570	1	1	1	3	
Ti I	5016.1613	0.848	-0.480	2	1	1	3	
Ti I	5210.3850	0.048	-0.820	2	1	1	1	
Ti I	5219.7000	0.021	-2.220	1	1	1	3	
Ti I	5223.6200	2.092	-0.490	2	1	1	2	
Ti I	5300.0107	1.053	-2.300	2	1	1	2	
Ti I	5426.2500	0.021	-2.950	1	1	1	2	
Ti I	5471.1926	1.443	-1.420	1	3	1	2	
Ti I	5689.4600	2.297	-0.360	1	1	1	2	
Ti I	5716.4500	2.297	-0.720	1	1	1	2	
Ti I	5866.4512	1.067	-0.790	1	1	1	3	
Ti I	5903.3149	1.067	-2.089	1	1	1	2	
Ti I	5918.5351	1.067	-1.640	1	1	1	2	



Doc. Title: The IWG7 4MOST Galactic Pipeline (4GP): Development Report 3										
Doc no.: MST-TNO-XXX-YYYYY-GGGG-HHHH										
Issue no.: 1.00						Date: 2018-06-11				
Document status						Page 37 of 40				

Ti I	5922.1092	1.046	-1.380	1	1	1	3	Cr II	5305.8526	3.827	-2.363	2	3	1	1
Ti I	5937.8089	1.067	-1.940	1	1	1	2	Cr II	5313.5628	4.074	-1.526	2	3	1	1
Ti I	5953.1596	1.887	-0.273	2	1	1	3	Mn I	4754.0400	2.282	-0.080	1	1	0	3
Ti I	6064.6262	1.046	-1.888	1	1	1	2	Mn I	4761.5100	2.953	-0.274	2	1	1	3
Ti I	6091.1713	2.267	-0.320	1	1	1	3	Mn I	4766.4200	2.920	0.105	2	1	1	3
Ti I	6126.2160	1.067	-1.368	1	1	1	3	Mn I	4783.4270	2.298	0.044	2	1	0	3
Ti I	6258.1015	1.443	-0.390	2	1	1	1	Mn I	5377.6073	3.844	-0.166	2	3	0	3
Ti I	6261.0975	1.430	-0.530	2	1	1	1	Mn I	5394.6698	0.000	-3.503	1	1	1	3
Ti I	6312.2359	1.460	-1.550	1	1	1	2	Mn I	5399.4745	3.853	-0.345	2	3	0	3
Ti I	6336.0985	1.443	-1.690	1	1	1	2	Mn I	5420.3508	2.143	-1.462	1	1	1	3
Ti I	6497.6838	1.443	-2.020	1	1	0	2	Mn I	5432.5392	0.000	-3.795	2	1	1	3
Ti I	6554.2229	1.443	-1.150	1	1	1	2	Mn I	6013.5100	3.072	-0.354	1	1	0	3
Ti I	6743.1221	0.900	-1.611	1	3	1	2	Mn I	6016.6700	3.073	-0.180	1	1	0	3
Ti III	4568.3140	1.224	-3.030	2	1	0	2	Mn I	6021.8200	3.075	-0.054	1	1	0	3
Ti III	4589.9580	1.237	-1.620	2	1	0	3	Fe I	4547.8470	3.547	-1.012	2	1	1	1
Ti III	4708.6621	1.237	-2.350	2	1	0	3	Fe I	4602.0007	1.608	-3.134	1	1	1	3
Ti III	4779.9850	2.048	-1.248	2	3	0	3	Fe I	4630.1200	2.279	-2.587	2	1	1	3
Ti III	4865.6114	1.116	-2.700	2	1	0	3	Fe I	4678.8457	3.603	-0.833	2	1	1	3
Ti III	4911.1948	3.124	-0.640	2	1	0	3	Fe I	4704.9478	3.686	-1.470	1	2	1	3
Ti III	5185.9018	1.893	-1.410	1	1	0	3	Fe I	4741.5294	2.832	-1.765	2	1	1	1
Ti III	5211.5304	2.590	-1.410	2	1	0	1	Fe I	4745.7998	3.654	-1.270	2	1	0	1
Ti III	5336.7710	1.582	-1.600	1	1	0	3	Fe I	4779.4391	3.415	-2.020	2	1	1	1
Ti III	5381.0150	1.566	-1.970	2	1	0	1	Fe I	4787.8266	2.998	-2.557	2	1	1	1
Ti III	5418.7510	1.582	-2.130	1	1	0	3	Fe I	4788.7566	3.237	-1.763	2	1	1	3
Ti II	6559.5637	2.048	-2.175	2	3	0	2	Fe I	4802.8800	3.642	-1.514	2	3	0	3
VI	4577.1741	0.000	-1.048	1	1	1	3	Fe I	4882.1431	3.417	-1.598	2	3	1	3
VI	5604.9312	1.043	-1.280	1	1	1	2	Fe I	4892.8589	4.218	-1.290	2	2	1	2
VI	5668.3608	1.081	-1.030	1	1	1	2	Fe I	4903.3099	2.882	-0.903	1	1	1	3
VI	5670.8527	1.081	-0.420	1	1	1	3	Fe I	4917.2299	4.191	-1.080	1	2	1	3
VI	5703.5750	1.051	-0.211	1	1	1	3	Fe I	4946.3880	3.368	-1.110	2	1	1	3
VI	5727.0480	1.081	-0.012	1	1	1	3	Fe I	4962.5716	4.178	-1.182	2	1	1	2
VI	5737.0589	1.064	-0.740	1	1	1	3	Fe I	4969.9173	4.218	-0.710	2	2	1	3
VI	6039.7219	1.064	-0.650	1	1	1	3	Fe I	4994.1295	0.915	-3.058	2	1	1	3
VI	6058.1390	1.043	-1.374	1	1	1	2	Fe I	5001.8633	3.882	-0.010	1	1	1	3
VI	6081.4410	1.051	-0.579	2	1	1	2	Fe I	5044.2108	2.851	-2.038	2	1	1	1
VI	6090.2139	1.081	-0.062	1	1	1	3	Fe I	5054.6425	3.640	-1.921	2	1	1	1
VI	6111.6445	1.043	-0.715	1	1	1	2	Fe I	5067.1495	4.220	-0.970	2	2	1	1
VI	6119.5233	1.064	-0.320	2	1	1	3	Fe I	5083.3382	0.958	-2.939	2	1	1	3
VI	6135.3608	1.051	-0.746	2	1	1	2	Fe I	5090.7731	4.256	-0.440	2	2	1	1
VI	6150.1565	0.301	-1.290	2	3	1	2	Fe I	5127.3592	0.915	-3.306	2	1	1	1
VI	6251.8273	0.287	-1.340	1	1	1	2	Fe I	5141.7389	2.424	-1.978	1	1	1	3
VI	6274.6488	0.267	-1.670	1	1	1	2	Fe I	5159.0576	4.283	-0.820	2	2	1	1
VI	6285.1499	0.275	-1.510	1	1	1	2	Fe I	5198.7108	2.223	-2.135	2	1	1	1
VI	6292.8251	0.287	-1.470	1	1	1	2	Fe I	5217.3893	3.211	-1.100	1	1	1	3
VI	6531.4146	1.218	-0.840	1	1	1	2	Fe I	5225.5260	0.110	-4.789	2	1	1	1
Cr I	4545.9530	0.941	-1.370	1	1	1	3	Fe I	5232.9400	2.940	-0.070	1	1	1	3
Cr I	4708.0130	3.168	0.070	2	1	1	3	Fe I	5242.4907	3.634	-0.967	1	1	1	3
Cr I	5296.6910	0.983	-1.360	1	1	1	3	Fe I	5243.7763	4.256	-1.050	2	1	1	3
Cr I	5300.7450	0.983	-2.000	2	1	1	3	Fe I	5250.2090	0.121	-4.933	1	1	1	3
Cr I	5348.3150	1.004	-1.210	1	1	1	3	Fe I	5250.6456	2.198	-2.180	2	1	1	1
Cr I	5719.8160	3.013	-1.580	2	1	1	2	Fe I	5253.4617	3.283	-1.573	2	1	1	1
Cr I	5783.0635	3.323	-0.375	1	3	1	3	Fe I	5288.5247	3.695	-1.490	2	1	1	1
Cr I	5783.8497	3.322	-0.295	2	3	1	3	Fe I	5293.9588	4.143	-1.770	2	2	1	3
Cr I	5787.9180	3.322	-0.083	1	3	1	3	Fe I	5295.3121	4.415	-1.590	2	2	1	3
Cr I	6330.0910	0.941	-2.787	1	3	1	3	Fe I	5302.3003	3.283	-0.720	2	1	1	3
Cr I	6537.9212	1.004	-3.718	2	3	0	2	Fe I	5322.0407	2.279	-2.802	1	1	1	3
Cr I	6630.0109	1.030	-3.560	2	3	1	2	Fe I	5364.8709	4.446	0.228	1	1	1	3
Cr II	4588.1990	4.071	-0.627	2	1	1	3	Fe I	5365.3987	3.573	-1.020	1	1	1	3
Cr II	5237.3285	4.073	-1.144	2	3	1	1	Fe I	5373.7086	4.473	-0.710	1	1	1	3



Doc. Title: The IWG7 4MOST Galactic Pipeline (4GP): Development Report 3											
Doc no.: MST-TNO-XXX-YYYYY-GGGG-HHHH											
Issue no.: 1.00						Date: 2018-06-11					
Document status						Page 38 of 40					

Fe I	5379.5736	3.695	-1.514	1	1	1	3	Fe I	6127.9062	4.143	-1.399	2	1	1	3
Fe I	5383.3685	4.313	0.645	1	1	1	3	Fe I	6137.6913	2.588	-1.402	2	1	1	3
Fe I	5386.3331	4.154	-1.670	1	2	1	3	Fe I	6151.6173	2.176	-3.295	1	1	1	3
Fe I	5389.4788	4.415	-0.410	2	2	1	1	Fe I	6157.7279	4.076	-1.160	1	2	0	3
Fe I	5398.2791	4.446	-0.630	1	2	1	3	Fe I	6165.3598	4.143	-1.473	1	1	1	3
Fe I	5415.1989	4.387	0.643	1	1	1	3	Fe I	6173.3343	2.223	-2.880	1	1	1	3
Fe I	5417.0332	4.415	-1.580	2	2	1	1	Fe I	6180.2026	2.728	-2.591	2	1	1	3
Fe I	5434.5235	1.011	-2.121	1	1	1	3	Fe I	6187.9892	3.943	-1.620	1	2	1	3
Fe I	5441.3387	4.313	-1.630	1	2	1	3	Fe I	6200.3125	2.609	-2.433	1	1	1	3
Fe I	5445.0420	4.387	-0.020	1	2	1	3	Fe I	6213.4294	2.223	-2.481	2	1	1	3
Fe I	5461.5495	4.446	-1.800	2	2	1	1	Fe I	6219.2805	2.198	-2.432	1	1	1	3
Fe I	5466.3958	4.371	-0.630	2	2	1	3	Fe I	6226.7342	3.884	-2.120	2	2	1	3
Fe I	5466.9880	3.573	-2.233	2	1	0	3	Fe I	6229.2259	2.845	-2.805	2	1	1	3
Fe I	5473.9005	4.154	-0.720	2	1	1	1	Fe I	6232.6403	3.654	-1.223	2	1	0	3
Fe I	5501.4649	0.958	-3.046	1	1	1	3	Fe I	6246.3180	3.603	-0.779	1	1	1	3
Fe I	5506.7787	0.990	-2.795	2	1	1	3	Fe I	6252.5549	2.404	-1.699	1	1	1	3
Fe I	5522.4461	4.209	-1.450	1	2	1	3	Fe I	6265.1323	2.176	-2.550	2	1	1	3
Fe I	5525.5436	4.231	-1.084	2	1	1	3	Fe I	6270.2234	2.858	-2.470	1	1	1	3
Fe I	5543.9356	4.218	-1.040	1	2	1	3	Fe I	6297.7926	2.223	-2.737	1	1	1	3
Fe I	5546.5058	4.371	-1.210	2	2	1	3	Fe I	6322.6850	2.588	-2.430	1	1	1	3
Fe I	5560.2115	4.435	-1.090	2	2	1	3	Fe I	6335.3299	2.198	-2.177	1	1	1	3
Fe I	5569.6180	3.417	-0.486	1	1	1	3	Fe I	6336.8234	3.686	-0.856	1	1	1	3
Fe I	5576.0888	3.430	-0.900	1	2	1	3	Fe I	6380.7432	4.186	-1.375	2	1	1	3
Fe I	5586.7555	3.368	-0.114	1	1	1	3	Fe I	6393.6004	2.433	-1.452	1	1	1	3
Fe I	5618.6323	4.209	-1.275	2	1	1	1	Fe I	6411.6480	3.654	-0.634	1	1	1	3
Fe I	5633.9461	4.991	-0.230	1	2	1	3	Fe I	6419.9487	4.733	-0.200	2	2	1	3
Fe I	5638.2621	4.220	-0.720	1	1	1	3	Fe I	6430.8450	2.176	-2.005	1	1	1	3
Fe I	5651.4689	4.473	-1.900	2	2	1	3	Fe I	6475.6239	2.559	-2.941	1	1	1	3
Fe I	5652.3176	4.260	-1.850	2	2	1	3	Fe I	6481.8698	2.279	-2.981	1	1	1	3
Fe I	5679.0229	4.652	-0.820	1	2	1	3	Fe I	6494.9804	2.404	-1.268	1	1	1	3
Fe I	5691.4970	4.301	-1.420	2	2	1	3	Fe I	6546.2381	2.759	-1.536	1	1	1	3
Fe I	5701.5442	2.559	-2.193	1	1	1	3	Fe I	6574.2266	0.990	-5.004	2	1	1	2
Fe I	5705.4642	4.301	-1.355	1	1	1	3	Fe I	6592.9124	2.728	-1.473	1	1	1	3
Fe I	5731.7618	4.256	-1.200	2	2	1	3	Fe I	6593.8695	2.433	-2.420	1	1	1	3
Fe I	5741.8477	4.256	-1.672	2	1	1	3	Fe I	6627.5438	4.549	-1.590	1	1	1	3
Fe I	5753.1223	4.260	-0.688	2	1	1	3	Fe I	6677.9851	2.692	-1.418	1	1	1	3
Fe I	5775.0805	4.220	-1.297	1	1	1	3	Fe I	6705.1009	4.607	-0.870	1	1	0	3
Fe I	5778.4530	2.588	-3.430	1	1	1	3	Fe I	6713.7425	4.796	-1.500	2	2	1	3
Fe I	5793.9147	4.220	-1.600	2	2	1	3	Fe I	6715.3818	4.608	-1.540	2	2	1	1
Fe I	5814.8071	4.283	-1.870	2	2	1	3	Fe I	6725.3558	4.103	-2.100	2	1	1	3
Fe I	5852.2187	4.549	-1.230	2	2	1	1	Fe I	6726.6663	4.607	-1.133	1	3	0	3
Fe I	5855.0758	4.608	-1.478	1	1	1	3	Fe I	6733.1503	4.638	-1.480	1	2	1	3
Fe I	5905.6712	4.652	-0.690	1	2	1	3	Fe I	6750.1515	2.424	-2.618	1	1	1	3
Fe I	5909.9724	3.211	-2.587	1	1	1	3	Fe I	6752.7066	4.638	-1.204	2	1	1	1
Fe I	5916.2473	2.453	-2.994	2	1	1	3	Fe I	6806.8429	2.728	-2.130	2	2	1	3
Fe I	5927.7887	4.652	-0.990	1	2	1	3	Fe I	6810.2622	4.607	-0.986	1	1	1	3
Fe I	5930.1799	4.652	-0.230	1	2	1	3	Fe I	6828.5912	4.638	-0.820	1	2	1	3
Fe I	5934.6545	3.929	-1.070	2	2	1	3	Fe I	6839.8300	2.559	-3.350	1	2	1	3
Fe I	5956.6940	0.859	-4.599	1	1	1	3	Fe I	6842.6853	4.638	-1.220	1	2	1	3
Fe I	5984.8150	4.733	-0.196	2	3	0	1	Fe I	6843.6554	4.549	-0.730	1	1	1	3
Fe I	5987.0648	4.796	-0.429	1	3	0	3	Fe I	6857.2493	4.076	-2.050	1	2	0	3
Fe I	6003.0111	3.882	-1.100	2	1	1	3	Fe I	6858.1483	4.608	-0.930	1	1	1	3
Fe I	6024.0575	4.549	-0.120	1	2	1	3	Fe I	7127.5676	4.988	-1.046	2	3	0	1
Fe I	6027.0508	4.076	-1.089	1	1	1	3	Fe I	7132.9863	4.076	-1.628	2	1	0	1
Fe I	6056.0046	4.733	-0.320	1	1	1	3	Fe I	7418.6668	4.143	-1.376	2	1	0	3
Fe I	6065.4820	2.609	-1.529	1	1	1	3	Fe I	7491.6474	4.301	-0.899	2	3	0	1
Fe I	6079.0077	4.652	-1.020	2	2	1	3	Fe I	7495.0656	4.220	-0.100	2	1	0	1
Fe I	6093.6429	4.608	-1.400	2	2	1	3	Fe I	7568.8987	4.283	-0.773	1	3	0	3
Fe I	6096.6641	3.984	-1.830	2	2	1	3	Fe I	7583.7881	3.018	-1.885	1	1	1	3



Doc. Title: The IWG7 4MOST Galactic Pipeline (4GP): Development Report 3											
Doc no.: MST-TNO-XXX-YYYYY-GGGG-HHHH											
Issue no.: 1.00							Date: 2018-06-11				
Document status							Page 39 of 40				

Fe I	7710.3632	4.220	-1.113	2	1	0	3	Ni I	6007.3098	1.676	-3.740	1	3	1	3
Fe I	7745.5133	5.086	-1.172	2	3	0	1	Ni I	6086.2815	4.266	-0.410	1	3	1	3
Fe I	7746.5954	5.064	-1.282	2	3	0	1	Ni I	6108.1158	1.676	-2.440	1	1	1	3
Fe I	7748.2693	2.949	-1.751	2	1	1	3	Ni I	6111.0703	4.088	-0.865	1	3	1	3
Fe I	7751.1090	4.991	-0.753	1	3	0	3	Ni I	6128.9731	1.676	-3.320	2	1	1	3
Fe I	7807.9090	4.991	-0.541	1	3	0	3	Ni I	6175.3665	4.089	-0.389	1	3	1	3
Fe I	7941.0879	3.274	-2.286	1	1	1	3	Ni I	6176.8070	4.088	-0.260	1	1	1	3
Fe II	4508.2803	2.856	-2.440	2	1	1	3	Ni I	6177.2415	1.826	-4.018	2	3	0	3
Fe II	4576.3400	2.844	-2.950	2	1	1	1	Ni I	6186.7109	4.105	-0.880	1	3	1	3
Fe II	4620.5128	2.828	-3.210	1	1	1	1	Ni I	6204.6000	4.088	-1.100	1	1	1	3
Fe II	4629.3390	2.807	-2.340	2	1	1	1	Ni I	6223.9810	4.105	-0.910	2	1	1	3
Fe II	4923.9212	2.891	-1.260	1	1	1	3	Ni I	6314.6585	1.935	-1.770	1	2	1	3
Fe II	4993.3502	2.807	-3.684	2	2	1	1	Ni I	6327.5985	1.676	-3.150	1	2	1	3
Fe II	5197.5675	3.231	-2.220	2	1	1	1	Ni I	6378.2470	4.154	-0.830	1	1	1	3
Fe II	5234.6226	3.221	-2.180	1	1	1	3	Ni I	6482.7983	1.935	-2.630	1	2	1	3
Fe II	5316.6087	3.153	-1.870	1	1	1	3	Ni I	6532.8730	1.935	-3.357	2	3	1	3
Fe II	5325.5523	3.221	-3.160	2	1	1	1	Ni I	6586.3098	1.951	-2.746	1	3	1	3
Fe II	5414.0698	3.221	-3.580	1	1	1	3	Ni I	6635.1224	4.419	-0.765	2	3	1	1
Fe II	5425.2485	3.199	-3.220	1	1	1	3	Ni I	6643.6303	1.676	-2.300	1	2	1	3
Fe II	5534.8380	3.245	-2.865	2	2	1	1	Ni I	6767.7720	1.826	-2.170	1	2	0	3
Fe II	5991.3709	3.153	-3.647	2	2	1	1	Ni I	6772.3149	3.658	-0.797	1	3	1	3
Fe II	6084.1017	3.199	-3.881	2	2	1	3	Ni I	6842.0367	3.658	-1.374	2	3	1	1
Fe II	6149.2459	3.889	-2.841	1	2	1	3	Ni I	7110.8961	1.935	-2.895	2	3	1	1
Fe II	6238.3859	3.889	-2.600	2	1	1	1	Ni I	7748.8843	3.706	-0.185	1	3	0	3
Fe II	6247.5569	3.892	-2.435	1	2	1	3	Ni I	7788.9299	1.951	-2.420	1	2	1	3
Fe II	6369.4590	2.891	-4.110	2	1	1	1	Ni I	7797.5798	3.898	-0.185	1	3	0	3
Fe II	6416.9190	3.892	-2.877	2	2	1	3	Cu I	5105.5370	1.389	-1.516	2	1	0	1
Fe II	6432.6800	2.891	-3.570	1	1	1	3	Cu I	5700.2373	1.642	-2.330	2	1	0	3
Fe II	6456.3796	3.903	-2.185	1	2	1	3	Cu I	5782.1269	1.642	-1.781	1	1	0	3
Fe II	6516.0766	2.891	-3.310	1	1	1	3	Zn I	4722.1530	4.030	-0.390	1	1	0	3
Fe II	7222.3912	3.889	-3.260	2	1	1	1	Zn I	4810.5280	4.078	-0.160	1	1	1	1
Fe II	7224.4778	3.889	-3.200	2	1	1	1	Sr I	4607.3310	0.000	0.283	1	1	0	3
Fe II	7711.7204	3.903	-2.500	1	1	1	3	Y II	4883.6821	1.084	0.265	1	3	0	3
Co I	4588.7294	0.432	-3.820	2	3	0	2	Y II	5087.4160	1.084	-0.170	1	1	0	1
Co I	4813.4764	3.216	0.120	1	3	0	3	Y II	5200.4060	0.992	-0.570	2	1	0	1
Co I	5301.0410	1.710	-1.940	2	1	1	2	Y II	5289.8150	1.033	-1.850	2	1	0	2
Co I	5331.4532	1.785	-1.990	1	1	1	3	Y II	5662.9241	1.944	0.384	2	3	0	3
Co I	5342.7006	4.021	0.741	2	3	0	1	Ba II	4554.0290	0.000	0.140	1	1	1	3
Co I	5352.0397	3.576	0.060	1	1	1	3	Ba II	4934.0760	0.000	-0.157	2	1	1	3
Co I	5647.2338	2.280	-1.560	1	1	1	3	Ba II	5853.6680	0.604	-0.907	1	1	1	3
Co I	6116.9902	1.785	-2.490	1	1	1	2	Ba II	6141.7130	0.704	-0.032	1	1	1	3
Co I	6454.9943	3.632	-0.250	2	1	1	2	Ba II	6496.8970	0.604	-0.407	1	1	1	3
Co I	6771.0343	1.883	-1.970	1	1	1	3	Eu II	6645.0940	1.380	0.120	1	1	0	3
Ni I	4831.1690	3.606	-0.321	2	1	1	3								
Ni I	4904.4118	3.542	-0.016	2	3	0	3								
Ni I	4953.2000	3.740	-0.580	2	1	1	1								
Ni I	5010.9381	3.635	-0.677	2	3	1	3								
Ni I	5035.3570	3.635	0.290	1	1	1	3								
Ni I	5082.3441	3.658	-0.439	2	3	1	1								
Ni I	5084.0957	3.679	-0.084	2	3	1	3								
Ni I	5084.0957	3.679	-0.084	2	3	1	3								
Ni I	5115.3922	3.834	-0.015	2	3	1	3								
Ni I	5578.7183	1.676	-2.640	1	1	1	3								
Ni I	5587.8578	1.935	-2.140	2	1	1	3								
Ni I	5593.7355	3.898	-0.682	1	3	1	3								
Ni I	5748.3507	1.676	-3.242	2	3	1	3								
Ni I	5805.2166	4.167	-0.579	1	3	1	3								
Ni I	5846.9935	1.676	-3.210	1	1	1	3								
Ni I	5996.7301	4.236	-1.037	2	3	1	3								

Table 10-1 Line list from Ruchti et al. (2015) [RD6].



Doc. Title: The IWG7 4MOST Galactic Pipeline (4GP): Development Report 3	
Doc no.: MST-TNO-XXX-YYYYY-GGGG-HHHH	
Issue no.: 1.00	Date: 2018-06-11
Document status	Page 40 of 40

Appendix D List of Acronyms

List of Acronyms	
4FS	4MOST Facility Simulator
4GP	4MOST Galactic Pipeline
4MOST	4-metre Multi-Object Spectroscopic Telescope
APOGEE	Apache Point Observatory Galactic Evolution Experiment
GALAH	The Galactic Archaeology with HERMES survey
HRS	High-Resolution Spectrograph
IWG	Infrastructure Working Group
LRS	Low-Resolution Spectrograph
RMS	Root mean square
RV	Radial velocity
SNR	Signal-to-noise ratio